Simulation Studies of 6 nm Free Electron Laser at the TESLA Test Facility Starting from Noise

E.L. Saldin [a], E.A. Schneidmiller [a], M.V. Yurkov [b]

[a] *Automatic Systems Corporation, 443050 Samara, Russia*

[b] *Joint Institute for Nuclear Research, Dubna, 141980 Moscow Region, Russia*

Abstract

The paper presents simulation results of Self-Amplified Spontaneous Emission (SASE) FEL at the TESLA Test Facility (TTF) at DESY. One-dimensional, time-dependent program package FEL1D was used for simulations. When simulating linear mode of operation, we have used actual number of electrons in the beam, $N \simeq 6 \times 10^9$, to calculate initial shot noise conditions at the undulator entrance. The results of linear simulations are compared with rigorous results of SASE FEL theory developed by R. Bonifacio et al. (Phys. Rev. Lett. **73**(1994)70). It was found that there is good agreement between simulation and analytical results. We also performed calculations of autocorrelation functions of the first and the second order, temporal and spectral characteristics of the output radiation of TTF FEL operating in linear and nonlinear SASE mode. These results could be of use for potential users to define the range of experiments which could be performed with SASE FEL radiation.

12 April 1996

1 Introduction

Self amplified spontaneous emission free electron laser (SASE FEL) is being planned to construct at the TESLA Test Facility at DESY [1]. One of the problems of the SASE FEL design consists in calculation of the output characteristics of such an FEL amplifier starting from noise. At present, only so called steady-state theory of an FEL amplifier is well developed. This theory describes the case when FEL amplifier amplifies electromagnetic radiation generated by external master oscillator. The amplitude and frequency of the input signal are controlled by experimenter. It is assumed that the signal of master oscillator has narrow bandwidth with respect to the bandwidth of the FEL amplifier. Under these initial conditions the amplitude of the amplified wave does not depend on time and depends only on coordinates. This was the main factor which has allowed to develop a wide range of reliable theoretical approaches for calculation of characteristics of conventional FEL amplifier (see, e.g. review papers [2–4]).

Steady-state theory of the FEL amplifier provides rather limited possibilities for precise description of SASE FEL [5,6]. Strictly speaking, the only rigorous result, provided with the steady state theory is calculation of characteristics of the beam radiation modes of the SASE FEL. Due to a high gain of SASE FEL at DESY, about 70 dB, the only TEM_{00} mode is survived having maximal gain. Characteristics of this mode do not depend on the nature of input signal and are determined by parameters of the FEL amplifier. So, it becomes possible to calculate field gain, transverse field distributions in Fresnel zone (i.e. inside the undulator) and directivity diagrams of radiation power in Fraunhofer diffraction zone (i.e. in experimental area) [5,6].

Temporal and spectral characteristics of SASE FEL output radiation are of great practical importance for potential users. Unfortunately, the steady state calculations allow only to estimate them. To obtain more specific information about temporal and spectral properties of SASE FEL radiation, three-dimensional, time-dependent codes should be used. At present, only one-dimensional theory of SASE FEL is relatively well developed [7,8]. In this paper we present the simulations of 6 nm option SASE FEL at DESY using one-dimensional, time-dependent codes constructed on the base of program package FEL1D [9].

The linear simulation code is based on the FEL equations written down in linear approximation. This code allows to perform rigorous simulation of initial conditions. When performing linear simulations of SASE FEL, we have used actual number of electrons in the TTF beam, $N \simeq 6 \times 10^9$, to calculate initial shot noise conditions at the undulator entrance. The results of linear simulations are compared with rigorous results of SASE FEL theory [7,8]. It was found that there is good agreement between simulation and analytical results. On the base of linear simulations we have estimated

the "effective" power of shot noise at the undulator entrance, which constituted the value about 100 W.

The nonlinear simulation code is based on macroparticle method. When performing nonlinear simulations we can not use actual number of the particles due to limited capabilities of computer. To overcome this problem, we have used technique proposed in ref. [10] when initial conditions are modelled with small number of macroparticles distributed by special method. The nonlinear simulation code also has been tested by means rigorous results of SASE FEL theory.

Using linear and nonlinear simulation codes we calculated autocorrelation functions of the first and the second order, temporal and spectral characteristics of the output radiation of TTF FEL operating in linear and nonlinear SASE mode. These results could be of use for potential users to define the range of experiments which could be performed with SASE FEL radiation.

2 Fluctuations of the beam current

In this paper we describe SASE mode of FEL operation using one-dimensional model and reasonable question arises how correctly such an approximation describes real processes occurring in SASE FEL at DESY. The answer on this question is positive. Indeed, we should remember that SASE FEL at DESY is a high gain device, providing power gain about 70 dB. Due to the high gain, the only fundamental TEM_{00} radiation mode is survived having maximal gain. It means that at sufficient undulator length there is total transverse coherence of the output radiation. On the other hand, one-dimensional model assumes that plane electromagnetic wave is amplified along the undulator which also has full transverse coherence. So, we can conclude that with an accuracy of some numerical factor of the order of unity the physics of FEL process in actual SASE FEL is described correctly with such a model.

In the case of SASE FEL there is no external electromagnetic wave at the undulator entrance, but from the very beginning there is modulation of the electron beam which is defined by shot noise in the electron beam. As we mentioned above, in SASE FEL at DESY the only fundamental TEM_{00} mode is survived which has full transverse coherence. It means, that when considering input shot noise, we should take into account only its fraction having full transverse coherence. The value of this initial modulation could be calculated as follows. Let us consider a monoenergetic electron beam with a current I_0. Then we remember that the electron current is constituted by moving electrons:

$$I(t) = (-e)\sum_k \delta(t - t_k) \ , \tag{1}$$

where $\delta(\ )$ is delta-function, (-e) is the charge of the electron and t_k is arrival time of the electron to the undulator entrance. It is seen that due to the random arrival of electrons, the value of the current fluctuates in time and only its value, averaged over an ensemble, will be equal to the mean value I_0. The beam current $I(t)$ and its Fourier transform $\bar{I}(\omega)$ are connected as follows:

$$I(t) = \frac{1}{2\pi} \int_{-\infty}^{\infty} \bar{I}(\omega) e^{-i\omega t} d\omega$$

$$\bar{I}(\omega) = \int_{-\infty}^{\infty} e^{i\omega t} I(t) dt = (-e) \sum_k e^{i\omega t_k} \ . \tag{2}$$

So, using this simple physical picture we can calculate the mean squared value of the Fourier harmonic, averaged over an ensemble (for $\omega \neq 0$):

$$<| \bar{I}(\omega) |^2> = < e^2 \sum_k \sum_j e^{i\omega(t_k - t_j)} > = e^2 \bar{N} \ , \tag{3}$$

where $\bar{N} = I_0 T/e$ is the average number of electrons passed through undulator entrance during the time interval T. It is important to notice that the double sum in eq. (3) is reduced to such a simple result due to the fact that time moments t_k are statistically independent. Expression (3) could be also written in the following form:

$$<| \bar{I}(\omega) |^2> = e I_0 T \ . \tag{4}$$

3 Rigorous results of SASE FEL theory

In the framework of one-dimensional model and when the effects of space charge field and energy spread in the beam could be neglected, an FEL operation could be described in terms of the gain parameter Γ and the efficiency parameter ρ (see, e.g. refs. [3,4]):

$$\Gamma = \left[\frac{2\pi^2 j_0 K^2 A_{JJ}^2}{I_A \lambda_w \gamma^3} \right]^{1/3}, \qquad \rho = \frac{\lambda_w \Gamma}{4\pi}, \tag{5}$$

where λ_w is the undulator period, $K = e\lambda_w H_w / 2\pi mc^2$ is the undulator parameter, H_w is the undulator magnetic field, j_0 is the beam current density, $(-e)$ and m are the electron charge and mass, $I_A = mc^3/e \simeq 17kA$, ω is the radiation frequency, $A_{JJ} = J_0(\nu) - J_1(\nu)$ and $\nu = K^2/(4 + 2K^2)$. In this paper all formulae are written for the case of a planar undulator.

In the previous section we have shown that due to shot noise there is density modulation of the electron beam at the undulator entrance. It follows from the steady-state theory of the FEL amplifier that if the electron beam modulated at frequency ω is fed to the undulator entrance, this initiates the amplification process of electromagnetic wave having the same frequency. One-dimensional model assumes that plane electromagnetic wave $E = \tilde{E}(z)\exp[i\omega(z/c - t)] + C.C.$ is amplified in the FEL amplifier. In the linear high-gain regime the amplitude of electromagnetic field grows exponentially with the undulator length:

$$\tilde{E}(z) \propto \exp[\Lambda z] \,, \tag{6}$$

where Λ is the growing root of eigenvalue equation ($\mathrm{Re}\,\Lambda > 0$):

$$\Lambda(\Lambda + iC)^2 = i\Gamma^3. \tag{7}$$

Here $C = [2\pi/\lambda_w - \omega(1 + K^2/2)/(2c\gamma^2)]$ is detuning of particle from resonance. Near the exact resonance, at $\mid C \mid \ll \Gamma$, we have the following solution for the growing root (see, e.g., ref. [4]):

$$\mathrm{Re}\,\hat{\Lambda} = \frac{\sqrt{3}}{2}(1 - \frac{\hat{C}^2}{9}), \qquad \mathrm{Im}\,\hat{\Lambda} = \frac{1}{2}(1 - \frac{4\hat{C}}{3}), \tag{8}$$

where $\hat{\Lambda} = \Lambda/\Gamma$, $\hat{C} = C/\Gamma = (\omega_0 - \omega)/2\rho\omega_0$ is detuning parameter and $\omega_0 = 4\pi c\gamma^2/[\lambda_w(1 + K^2/2)]$ is resonant frequency.

The solution of initial-value problem in a high-gain limit for the case when modulated electron beam is fed to the entrance of a planar undulator has the form (see, e.g. [4], Appendix B):

$$\frac{\bar{E}(\omega, \hat{z})}{E_0} = \frac{1}{3}\exp\left[\frac{\sqrt{3}}{2}(1 - \frac{\hat{C}^2}{9})\hat{z}\right]\frac{\bar{j}(\omega)}{j_0} \,, \tag{9}$$

where $\bar{E}(\omega, z)$ and $j(\omega)$ are, respectively, Fourier components of electric field of the wave $E(t, z)$ and of the beam current density $j(t)$ at the undulator entrance. Normalizing factors E_0 and j_0 are given with the expressions:

$$E_0 = 8\pi\rho^2\gamma^2 I_A/(\lambda_w c K A_{JJ}) \,, \qquad j_0 = I_0/S \,,$$

where S is the transverse area of the electron beam. We have mentioned above that transversely coherent fraction of input shot noise is defined by the total beam current,

so

$$\frac{\bar{j}(\omega)}{j_0} = \frac{\bar{I}(\omega)}{I_0} \,. \tag{10}$$

The radiation pulse energy, averaged over an ensemble is defined as

$$< W >= \frac{cS}{4\pi} \int_0^T < E^2(t,z) > dt = \frac{cS}{4\pi^2} \int_0^\infty <\mid \bar{E}(\omega,z) \mid^2> d\omega. \tag{11}$$

Substituting eqs. (9) and (10) into eq. (11) and taking into account eq. (4), we can calculate the radiation power $\bar{P}_{\rm out} =< W > /T$ averaged over an ensemble and the normalized efficiency $\hat{\eta} = \bar{P}_{\rm out}/\rho P_{\rm b}$ [11]:

$$\hat{\eta} = \frac{\sqrt{4\pi\rho}}{3\sqrt{\sqrt{3}\hat{z}N_\lambda}} \exp[\sqrt{3}\hat{z}] \,, \tag{12}$$

where $P_{\rm b} = \gamma mc^2 I/e$ is the electron beam power, $\hat{z} = \Gamma z$ and $N_\lambda = 2\pi I/e\omega_0$.

It follows from eq. (11) that the spectral density of the radiation energy is proportional:

$$\frac{d < W >}{d\omega} = \frac{cS}{4\pi^2} <\mid \bar{E}(\omega,z) \mid^2> \propto \exp[\sqrt{3}\hat{z}(1 - \hat{C}^2/9)] \,. \tag{13}$$

So, we can write the expression for the spectrum bandwidth (half width at half maximum) of the SASE FEL [12]:

$$\left.\frac{\Delta\omega}{\omega_0}\right|_{HWHM} = 6\sqrt{\frac{\ln 2}{\sqrt{3}}}\frac{\rho}{\sqrt{\hat{z}}} \,, \tag{14}$$

The value of the ρ parameter is much less than unity, so it follows from expression (14) that SASE FEL selects only narrow frequency band from input "white" noise. As a result, there is some correlation in time in the output signal. To describe correlation phenomena, the notion of autocorrelation function is introduced. The first order autocorrelation function is defined as:

$$B_1(\tau,z) = \frac{< \tilde{E}(t,z)\tilde{E}^*(t+\tau,z) + C.C. >}{2 <\mid \tilde{E}(t,z) \mid^2>}. \tag{15}$$

For the narrow band linear system with symmetric frequency characteristic, the first order autocorrelation function could be written in the form:

$$B_1(\tau,z)=\frac{\int\limits_{-\infty}^{\infty} d(\Delta\omega)<|\bar{E}(z,\Delta\omega)|^2>\cos[(\Delta\omega)\tau]}{\int\limits_{-\infty}^{\infty} d(\Delta\omega)<|\bar{E}(z,\Delta\omega)|^2>}, \tag{16}$$

where $\Delta\omega=\omega-\omega_0$. Taking into account eq. (13) we finally obtain the first order autocorrelation function for the output radiation of the FEL amplifier starting from noise:

$$B_1(\hat{\tau})\propto\int\limits_{-\infty}^{\infty}\exp\left[\sqrt{3}\hat{z}(1-\hat{C}^2/9)\right]\cos(2\hat{C}\hat{\tau})d\hat{C}\propto\exp\left[-9\hat{\tau}^2/\sqrt{3}\hat{z}\right], \tag{17}$$

where $\hat{\tau}=\rho\omega_0\tau$. It should be noticed that when writing down eqs. (16) and (17) we used an assumption that the bandwidth of the linear system is small with respect to the value of ω_0 which allows one to extend the lower limit of integration over $\Delta\omega$ from $-\omega_0$ to $-\infty$.

Defining the autocorrelation time $\hat{\tau}_{1/2}$ by the condition of decreasing of the first order autocorrelation function by factor of 2, we get [13]:

$$\hat{\tau}_{1/2}=\frac{\sqrt{\hat{z}}}{3}\sqrt{\sqrt{3}\ln 2} \tag{18}$$

So, we can conclude that the output radiation of SASE FEL has appearance of wavepackets series (or spikes [7,8]). The length of each wavepacket is about $c\tau_{1/2}$ and there is no correlation between wavepackets. These wavepackets move with respect to the electron beam with relative velocity v_g-v_z, where $v_g=d\omega/d\kappa$ is group velocity of wavepacket and v_z is the longitudinal velocity of electrons. Remembering that $\kappa=\omega/c+\mathrm{Im}\,\Lambda$ (see eqs. (6) and (8)), we obtain [8]:

$$v_g=c\left[1+\frac{1}{2\gamma_z^2}\frac{d\,\mathrm{Im}\,\hat{\Lambda}}{d\hat{C}}\right]=c\left[1-\frac{1}{3\gamma_z^2}\right],$$

where $\gamma_z^2=\gamma^2/(1+K^2/2)$. It is interesting to notice that spikes slip along beam three times slower than normal slippage rate $c-v_z=c/2\gamma_z^2$.

To obtain more specific notion about properties of output radiation, one should perform numerical simulations of start-up from noise. Nevertheless, analytical results, obtained in this section, serve as a primary standard for testing of numerical codes.

4 Method for time-dependent simulation

Time-dependent algorithm for simulation of FEL amplifier should take into account the slippage effect which connected with the fact that electromagnetic wave moves with the velocity of light c, while the electron beam moves with longitudinal velocity v_z. Electron motion in the undulator is a periodic one, so the radiation of each electron $E(z,t)$ is also periodic function:

$$E(z,t) = f(z-ct) = f(z-ct+\lambda) \ ,$$

with period

$$\lambda = \lambda_w \frac{c-v_z}{v_z} \simeq \frac{\lambda_w}{2\gamma_z^2} = \lambda_w \frac{1+K^2/2}{2\gamma^2}. \tag{19}$$

It seems to be natural to construct the following algorithm [7,8]. Suppose, we have electron bunch of length l_b. We divide this length into $N_b = l_b/\lambda$ boxes. FEL equations are used in each box for calculation of the motion of the electrons and evolution of the radiation field within one undulator period, i.e. within $\Delta\hat{z} = \lambda_w\Gamma$. The using of steady-state FEL equations averaged over undulator period is justified by the fact that FEL amplifier is resonance device with a narrow bandwidth (see eq. (14) remembering that $\rho \ll 1$). Then we should take into account the slippage effect, i.e. that electromagnetic radiation advances the electron beam by the wavelength λ while electron beam passes one undulator period. It means that radiation which interacted with electrons in the j th box slips to the electrons located in the next, $j+1$ th box. Then procedure of integration is repeated, etc.

This algorithm allows us to calculate the values of radiation field for each box as function of longitudinal coordinate z. Time dependence of the radiation field has the form:

$$E(z,t) = \tilde{E}(z,t)e^{-i\omega_0(z/c-t)} + C.C. \tag{20}$$

at any position along the undulator. Here we explicitly segregated slowly varying complex amplitude $\tilde{E}(z,t)$. Remembering that at any fixed point z of the undulator, time interval between the arrival of radiation connected with to adjacent boxes is equal to $\Delta t = t_{j+1} - t_j = \lambda/c$, we have discrete representation of $\tilde{E}(z,t_j)$.

Spectral characteristics of output radiation are of great practical importance. To calculate them, we use Fourier transform:

$$E(z,t) = \frac{1}{2\pi}\int_{-\infty}^{\infty} \bar{E}(z,\omega)e^{-i\omega t}d\omega$$

$$\bar{E}(z,\omega) = \int_{-\infty}^{\infty} e^{i\omega t}[\tilde{E}(z,t)e^{-i\omega_0 t} + C.C.]dt\ . \tag{21}$$

Taking into account that the radiation field $E(z,t)$ is calculated in discrete moments, we obtain:

$$\bar{E}(z,\omega) = \frac{2\pi}{\omega_0}\sum_j \tilde{E}^{(j)}e^{-2\pi i j\Delta\omega/\omega_0},$$

where $\Delta\omega = \omega - \omega_0$ and $\omega > 0$.

The spectral density of radiation energy is given by the expression:

$$\frac{dW}{d(\Delta\omega)} = \frac{cS}{4\pi^2}\bar{E}(z,\Delta\omega)\bar{E}^*(z,\Delta\omega)\ , \tag{22}$$

which is related with the total radiation energy in the pulse as:

$$W = \frac{cS}{4\pi}\int_0^T E^2(z,t)dt = \int_{-\infty}^{\infty}\frac{dW}{d(\Delta\omega)}d(\Delta\omega)\ , \tag{23}$$

The first and the second order autocorrelation functions, $B_1(\tau)$ and $B_2(\tau)$, are calculated in accordance with the definitions:

$$B_1(\tau,z) = \frac{\int_0^T dt\tilde{E}(t,z)\tilde{E}^*(t+\tau,z) + C.C.}{2\int_0^T dt\tilde{E}(t,z)\tilde{E}^*(t,z)}\ ,$$

$$B_2(\tau,z) = \frac{T\int_0^T dt\ |\ \tilde{E}(t,z)\ |^2|\ \tilde{E}(t+\tau,z)\ |^2}{\left[\int_0^T dt\ |\ \tilde{E}(t,z)\ |^2\right]^2}\ . \tag{24}$$

5 Parameters of 6 nm option of SASE FEL

General design of 6 nm option of SASE FEL at DESY is presented in ref. [1]. The driving beam for SASE FEL will be produced by 1 GeV superconducting linear

Table 1
Parameters of TTF FEL / 6 nm option /

Electron beam	
Energy, $\mathcal{E}_0$	1000 MeV
Charge in the bunch	1 nC
Peak current, I_0	2500 A
rms bunch length, σ_z	5×10^{-3} cm
Normalized rms emittance , ϵ_n	2×10^{-4} cm rad
External β-function,	300 cm
rms beam size in the undulator, σ_r	5.5×10^{-3} cm
Bunch separation	111 ns
Number of bunches per train	7200
Repetition rate	10 Hz
Undulator	
Type	Planar
Period, λ_w	2.73 cm
Peak magnetic field, H_w	4.97 kGs
Radiation	
Wavelength, λ	6.42 nm
Reduced parameters	
Gain parameter, Γ	9.7×10^{-3} cm^{-1}
Efficiency parameter, ρ	2.1×10^{-3}

accelerator [14]. The required value 2.5 kA of peak current will be achieved after three sequential stages of bunch compression. The undulator will be a hybrid permanent magnet one with a total length up to 30 m. To keep the beam size small in the undulator, additional focusing (FODO-lattice) will be used. Parameters of the FEL have been optimized using steady-state theory [5,6]. Design parameters of the SASE FEL at DESY are presented in Table 1.

The transverse phase space distribution of the particles in the beam is assumed to be gaussian and the beam is matched with the magnetic system of the undulator. The beam current density is given by the expression:

$$j(r,s) = \frac{I(s)}{2\pi\sigma_r^2}\exp(-r^2/2\sigma_r^2), \tag{25}$$

where $\sigma_r = \sqrt{\epsilon_n \beta/\gamma}$, $I(s)$ is the beam current, $s = z - v_z t$, ϵ_n is the normalized emittance, β is the beta function and γ is the relativistic factor.

In the present study we consider two models of axial distribution of the beam current, stepped profile with $I(s) = I_0$ and length $l_b = \sqrt{2\pi}\sigma_z$ and gaussian profile with $I(s) = I_0 \exp(-s^2/2\sigma_z^2)/\sqrt{2\pi}\sigma_z$, where I_0 is the peak beam current (see Table 1). When writing down 1-D FEL equations, we substitute the beam current density by effective value $j(s) = I(s)/(2\pi\sigma_r^2)$. It means that the actual beam with transverse gaussian distribution of the beam current density is modelled by the electron beam with constant (along transverse direction) beam current density having transverse area $S = 2\pi\sigma_r^2$.

6 Linear mode of operation

In sections 5 and 6 we present description of time-dependent algorithms. All formulae, presented below, are written for the case of stepped axial profile of electron beam. Extending of these formulae to the case of an arbitrary gradient axial profile could be performed in a simple manner.

When performing numerical simulations, we neglect the effects of space charge and longitudinal velocity spread in the beam. The length of the electron beam l_b is assumed to be rather large, $l_b \gg (1 + K^2/2)/(2\gamma^2\Gamma)$. We also assume that fluctuations of the beam current density define the value of input shot noise signal. It means that we neglect the effect of the longitudinal velocity fluctuations connected with finite energy spread in the beam. One can show that the ratio of the noise signal due to the fluctuations of the velocity to the shot noise signal is of the order of $\sigma_E^2/\mathcal{E}^2\rho^2$, where σ_E is the energy spread in the beam. This ratio is always less than unity, because the safety margin of FEL amplifier assumes that $\sigma_E^2/\mathcal{E}^2 \ll \rho^2$.

Linear time-dependent simulation algorithm is organized as follows. We divide the electron beam into $N_b = l_b/\lambda$ boxes. Linear steady-state FEL equations are used in each box for calculation of the evolution of the radiation field within one undulator period, i.e. within $\Delta\hat{z} = \lambda_w\Gamma$ (see, e.g. [4]):

$$\frac{d^3\hat{E}^{(j)}}{d\hat{z}^2} = i\hat{E}^{(j)} , \tag{26}$$

where $\hat{E}^{(j)} = \tilde{E}/E_0$ is reduced electric field of electromagnetic wave in the j th box and $E_0 = 8\pi\rho^2\gamma^2 I_A/(\lambda_w c K A_{JJ})$. Here we assume that electron beam is monoenergetic. Simulation of time-dependent effects is performed with the algorithm described in

section 4. When constructing numerical simulation code, it is more convenient to rewrite eq. (26) in the following form:

$$\frac{d^2 a_1^{(j)}}{d\hat{z}^2} = i\hat{E}^{(j)} , \qquad \frac{d\hat{E}^{(j)}}{d\hat{z}} = a_1^{(j)}, \tag{27}$$

To find the evolution of the beam bunching $a_1^{(j)}$ and electromagnetic field, we should define initial conditions at the undulator entrance at $\hat{z} = 0$. At the entrance of the undulator there is no radiation field and fluctuations of the beam current density caused by shot noise in the electron beam play the role of input signal. If total number of the particles is equal to N, then the number of particles per one box is equal to $N_\lambda = N/N_b$. To calculate initial conditions, we distribute N_λ particles randomly in each box. Amplitude and phase of the beam bunching are calculated in accordance with relation:

$$\begin{aligned} a_1^{(j)}|_{\hat{z}=0} &= N_\lambda^{-1} \sum_{k=1}^{N_\lambda} \exp(-i\psi_k^{(j)}) \\ \frac{da_1^{(j)}}{d\hat{z}}|_{\hat{z}=0} &= 0 , \end{aligned} \tag{28}$$

where $\psi_k^{(j)} = 2\pi s_k^{(j)}/\lambda$ is the electron phase and $s_k^{(j)}$ is axial coordinate of the particle in the bunch. The initial condition on the derivative of the density modulation has been set equal to zero, because the effect of the velocity fluctuations at the undulator entrance could be neglected as we discussed above.

In Figs.1-4 and in Figs.5-6 we present the results of numerical simulations of linear regime for stepped and gaussian axial profile of the electron beam, respectively. To calculate initial conditions at the undulator entrance, we used actual number of electrons in the TTF beam, $N \simeq 6 \times 10^9$.

Fig.1 present the plots of temporal structure of radiation pulse power at $z = 12$ m for stepped axial profile of electron beam. It is seen that the radiation has appearance of sequence of spikes. In Fig.2 we present spectral distribution of radiation power. Fig.3 presents the plot of the first order autocorrelation function $B_1(\tau)$. One can easily obtain that half width of autocorrelation function is in good agreement with analytical estimation given by eq. (18). Fig.4 presents the plot of the second order autocorrelation function $B_2(\tau)$.

When simulating SASE FEL with steady-state codes, the notion of "effective" power of input signal is usually introduced. As in the linear high gain limit the average power of FEL amplifier grows exponentially with undulator length, we can write (see, e.g.

[4]):

$$P_{\rm out} = \frac{1}{9} P_{\rm in} \exp(\sqrt{3}\hat{z}) \ . \tag{29}$$

The value of $P_{\rm in}$ could be obtained in the following way. First, at fixed undulator length, we should perform averaging of output power over the total length of the electron. Then, using eq. (29) we can obtain the value of $P_{\rm in}$. Calculations, have been performed at the undulator length of 12 m and provided the value of$P_{\rm in} \simeq 100$ W. It is interesting to compare this value with analytical estimation. Using relation (12), we can obtain estimation for "effective" power of input signal of TTF FEL: $P_{\rm in} \simeq 3\rho^2 P_{\rm b}/N_\lambda \simeq 100$ W (here we have taken into account that $\hat{z} \simeq 11$ at the length of undulator 12 m). So, we see that analytical estimation for "effective" input power provides good accuracy.

It follows from the results of numerical simulations that all the important characteristics of radiation (dependence of radiation power averaged over the bunch on the longitudinal coordinate, autocorrelation time, group velocity of wavepackets, etc.) are in a good agreement with the analytical asymptotics presented in Section 3. Typical difference of the order of 10 % can be explained by finite number ($\sim 10^2$) of wavepackets (spikes) inside the radiation pulse of TTF FEL. The reason is that these spikes are uncorrelated and uncertainty in the above mentioned characteristics must be inversly proportional to the square root of the number of this statistically independent processes (see, e.g. [8]). In particular, this effect explain an oscillating behavior around zero value of the tails of autocorrelation functions. In the asymptotics of infinitely long electron bunch one would get the exact correspondence with the analytical results.

Similar dependencies for the case of gaussian axial profile of electron beam are presented in Figs.5 – 6. One can get impression about the influence of the bunch shape on the temporal and spectral characteristics of radiation in linear mode of operation of SASE FEL.

It should be noted that presented in this section algorithm does not exhaust all the possibilities to calculate the linear mode of SASE FEL operation and method based on Green's function technique could be used, too. In a linear system spectrum of output signal is defined by the frequency characteristic of the system and the spectrum of input signal. In the case under study this could be written in the following form:

$$\bar{E}(z,\omega) = G(z,\omega)\bar{j}(\omega) \ , \tag{30}$$

where $G(z,\omega)$ is the frequency characteristic of the system (Green's function) and $\bar{E}(z,\omega)$ and $\bar{j}(\omega)$ are, respectively, Fourier components of output electric field and

input beam current. The Green's function could be obtained solving linear equations of FEL amplifier at given initial conditions at the undulator entrance (see, e.g. refs. [7,8]). In the case under study initial conditions assume that modulated electron beam is fed to the undulator entrance (one can obtain that we used particular expression for the Green's function in eq. (9), written down for a high-gain limit). The calculations of the initial noise spectrum of the beam current density could be performed using eq. (2). Then, using eq. (9) we can calculate the spectrum of output radiation. The knowledge of $\bar{E}(z,\omega)$ allows one to calculate energy spectrum and autocorrelation function and to reconstruct temporal structure of radiation pulse (see eqs. (22), (24) and (21)). Both algorithms (based on the Green's function technique and time-dependent) provide identical results. In this paper we have used the time-dependent algorithm, because it could be naturally extended to the nonlinear case.

7 Nonlinear mode of operation

Nonlinear time-dependent simulation algorithm is based on similar technique described in the previous sections. We divide the electron beam into $N_b = l_b/\lambda$ boxes. Steady-state FEL equations are used in each box for calculation of the motion of the electrons and evolution of the radiation field within one undulator period, i.e. within $\Delta\hat{z} = \lambda_w\Gamma$ (see, e.g. [4]):

$$\begin{aligned} d\hat{P}_k^{(j)}/d\hat{z} &= -\hat{E}^{(j)}\exp(i\psi_k^{(j)}) + C.C., \\ d\psi_k^{(j)}/d\hat{z} &= \hat{P}_k^{(j)} \ , \end{aligned} \tag{31}$$

$$d\hat{E}^{(j)}/d\hat{z} = a_1^{(j)} \tag{32}$$

where $j = 1,\dots N_\lambda$, $k = 1,\dots M$ and M is the number of macroparticles in each box and $\hat{P}_k^{(j)} = \omega(\mathcal{E}_k^{(j)} - \mathcal{E}_0)/(c\gamma_z^2\mathcal{E}_0\Gamma)$ is reduced energy deviation from nominal value. Amplitude and phase of the beam bunching are calculated as follows:

$$a_1^{(j)} = M^{-1}\sum_{k=1}^{N_\lambda}\exp(-i\psi_k^{(j)}) \tag{33}$$

where $\psi_k^{(j)}$ is the electron phase.

To take into account slippage effect, we transfer radiation which interacted with electrons in the j th box into $j+1$ th box after each undulator period.

It should be noticed that there is one principal distinction with respect to the case of linear simulations. Namely, we used actual number of the particles in the TTF bunch to calculate initial conditions for linear code. In the case of nonlinear simulations we can not use actual number of the particles due to limited capabilities of computer. To overcome this problem, we have used technique proposed in ref. [10]. We choose the number of macroparticles in each box to be equal to $M \ll N_\lambda$. The particles are distributed over phase ψ in the following way:

$$\psi_k^{(j)} = \frac{2\pi}{M}(k - \frac{1}{2}) + (2F_0^1 - 1)\delta \ , \tag{34}$$

where F_0^1 is a pseudo-random variable uniformly distributed between 0 and 1 and $\delta = \sqrt{3M/N_\lambda}$.

In Figs.7 – 15 and Figs.16 – 24 we present the results of nonlinear simulations of TTF FEL for stepped and gaussian axial profile of the electron beam, respectively. The number of macroparticles in each box was equal to $M = 20$. Spectral distribution of radiation power has been calculated in the same way as it was described in Section 4.

These plots allow one to trace the dependence of the output characteristics of TTF FEL on the undulator length. Here we state only the common features. First, temporal structure of the radiation becomes to be more cut up. Second, the radiation spectrum is broadened after saturation point and spreads to lower frequencies which is connected with visible beam energy losses. Third, the output radiation power continues to grow after saturation point. Comparison of the plots presented in Figs.7 – 15 and Figs.16 – 24 shows that in the case of TTF FEL output characteristics of radiation do not depend significantly on the form of the longitudinal distribution of the beam current.

Acknowledgement

The authors should like to thank R. Bonifacio, J. Rossbach and P. Pierini for many useful discussions and recommendations. We thank G. Materlik and J. Schneider for their interest in our work.

References

[1] "A VUV Free Electron Laser at the TESLA Test Facility: Conceptual Design Report", DESY Print TESLA-FEL 95-03, Hamburg, DESY, 1995.

[2] Laser Handbook, Vol.6, Free Electron Lasers (edited by W.B. Colson et al, North Holland, Amsterdam, 1990).

[3] R. Bonifacio et al., Riv. Nuovo Cimento, Vol. **13**, No. 9 (1990).

[4] E.L. Saldin, E.A. Schneidmiller and M.V. Yurkov, Phys. Rep. **260**(1995)187.

[5] E.L. Saldin, E.A. Schneidmiller and M.V. Yurkov, DESY Print May 1995, TESLA-FEL 95-02, Hamburg, DESY, 1995.

[6] W. Brefeld et al., "Parameter study of the VUV FEL at the TESLA Test Facility", Presented at 17th International Free Electron Laser Conference (New York, August 1995).

[7] R. Bonifacio et al., Nucl. Instrum. and Methods **A341**(1994)181.

[8] R. Bonifacio et al., Phys. Rev. Lett. **73**(1994)70.

[9] E.L. Saldin, E.A. Schneidmiller and M.V. Yurkov, Sov. J. Part. Nucl. **23**(1992)104.

[10] C. Penman and B.W.J. McNeil, Opt. Commun. **90**(1992)82.

[11] K.J. Kim, Phys. Rev. Lett. **57**(1986)1871.

[12] A.M. Kondratenko and E.L. Saldin, Part. Acc. **10**(1980)207.

[13] P. Pierini and W. Fawley, "Shot Noise Startup of the 6 nm SASE FEL at the TESLA Test Facility", Presented at 17th International Free Electron Laser Conference (New York, August 1995).

[14] "A VUV Free Electron Laser at the TESLA Test Facility: Conceptual Design Report", DESY Print TESLA-FEL 95-03, Hamburg, DESY, 1995.

(a)

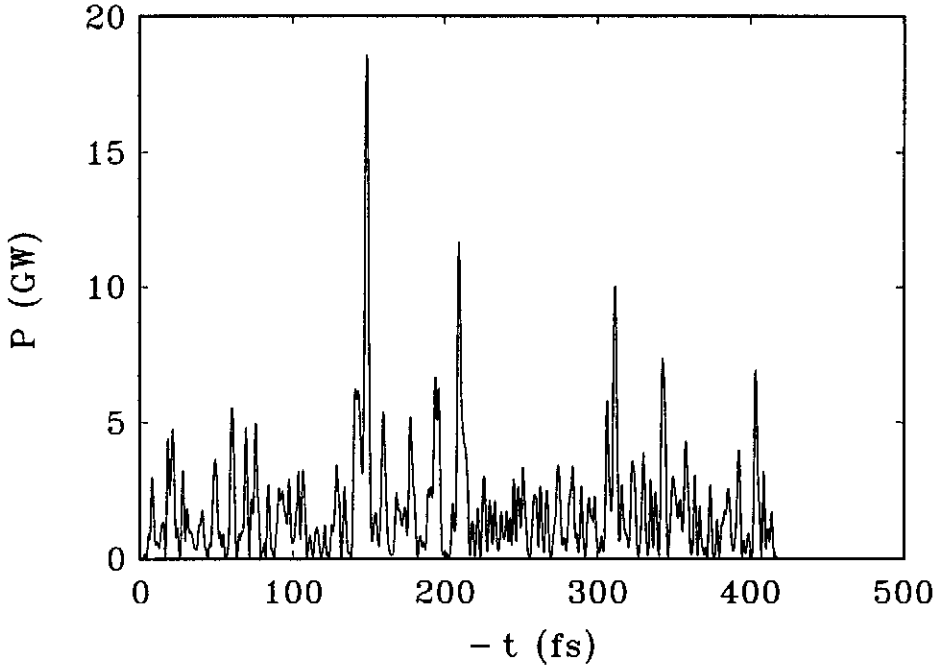

(b)

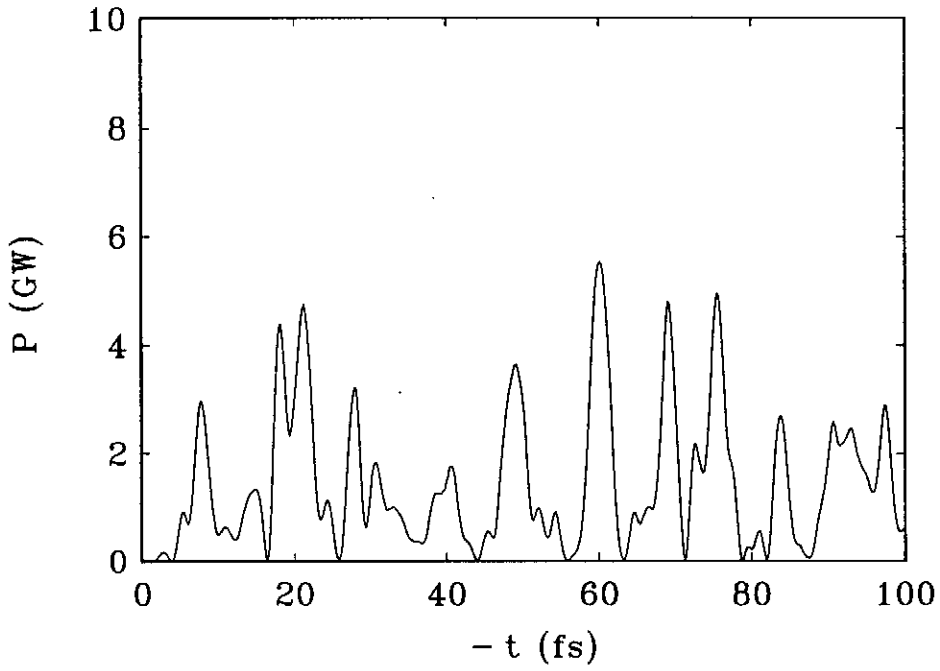

Fig. 1. Temporal structure of radiation pulse at $z = 12$ m for stepped axial profile of electron beam. Graph (a) is plotted over the full length of the electron beam and graph (b) presents enlarged fraction of graph (a). Calculations have been performed with linear simulation code.

(a)

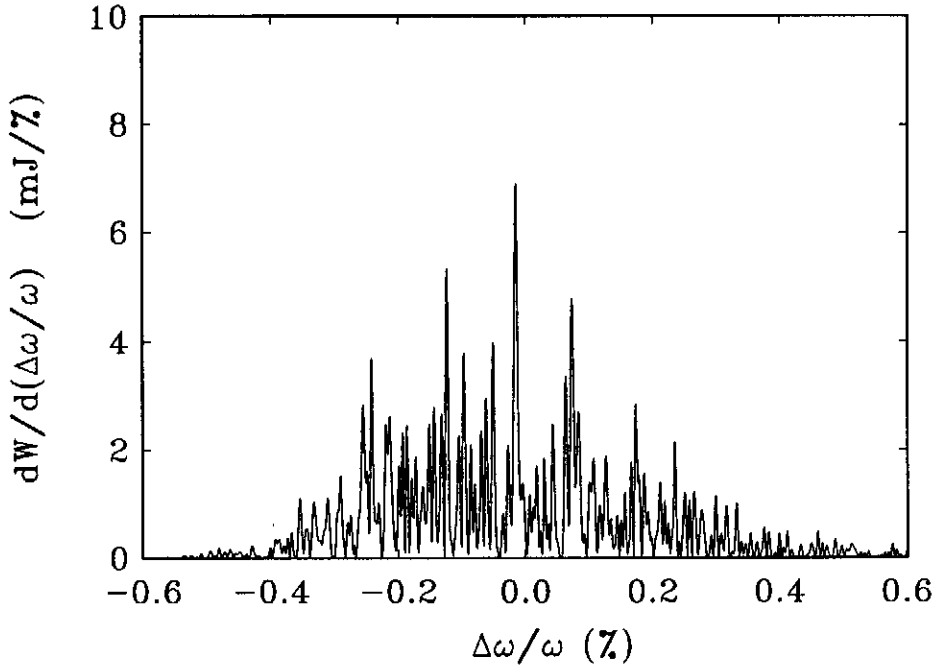

(b)

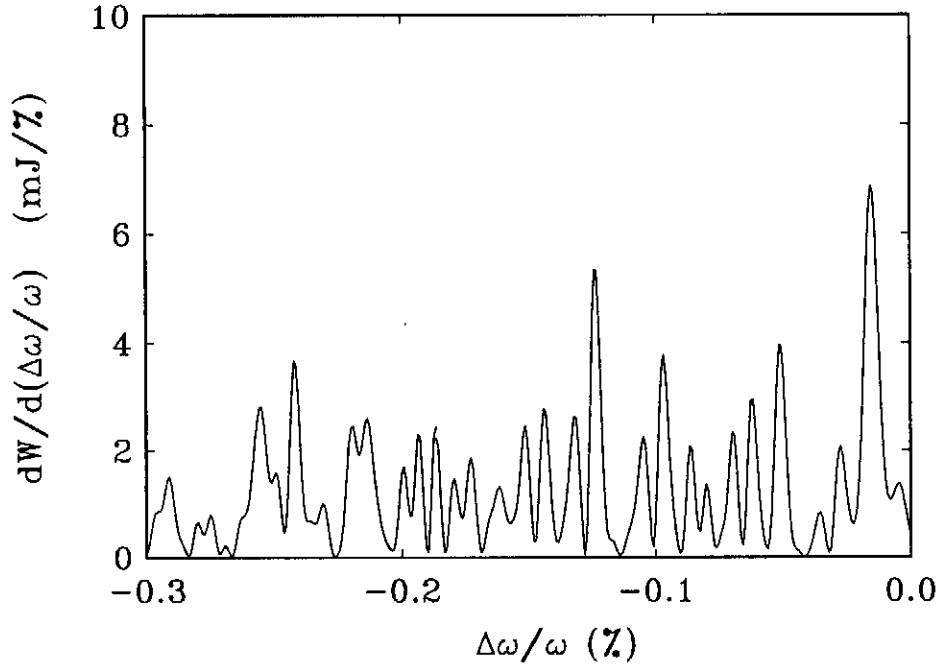

Fig. 2. Spectrum of radiation pulse at $z = 12$ m for stepped axial profile of electron beam. Graph (a) is plotted over the full length of the electron beam and graph (b) presents enlarged fraction of graph (a). Calculations have been performed with linear simulation code.

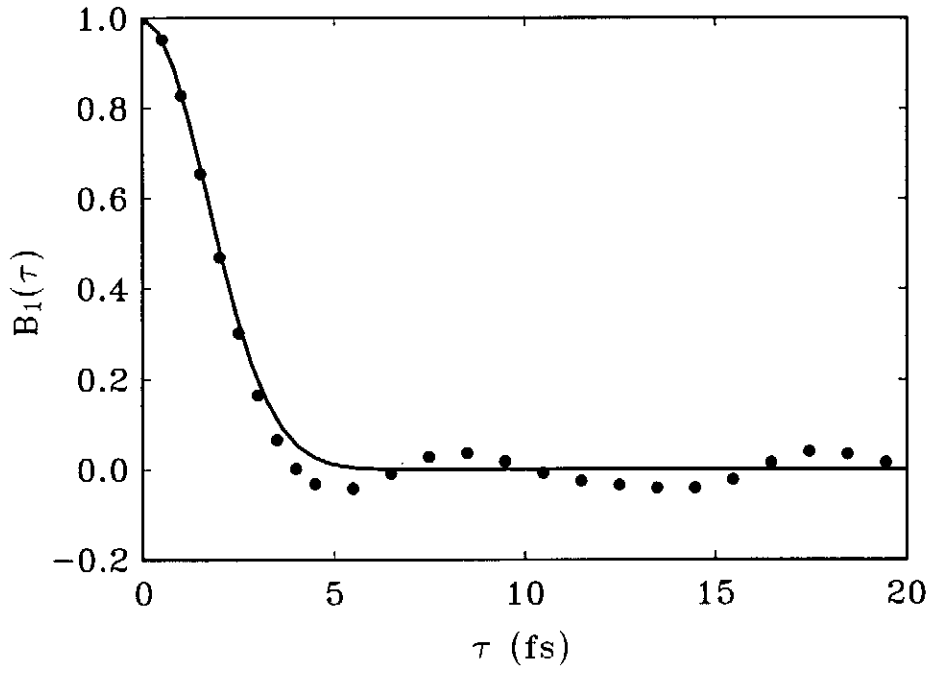

Fig. 3. First order autocorrelation function $B_1(\tau)$ of output radiation pulse at $z = 12$ m for stepped axial profile of electron beam. Circles are the results of calculations with linear simulation code and solid curve is calculated with analytical formula (16).

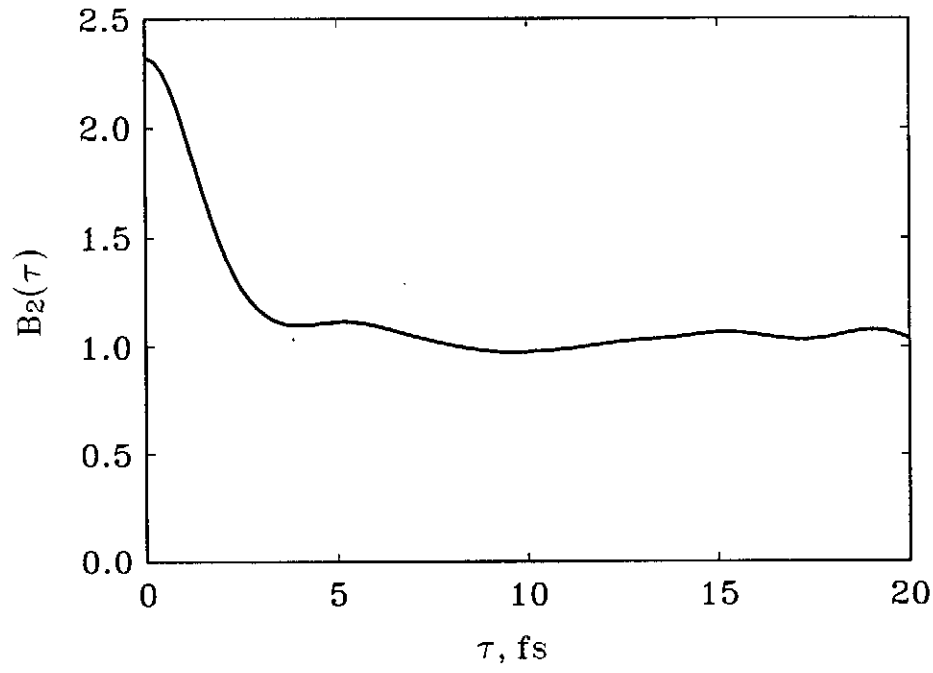

Fig. 4. Second order autocorrelation function $B_2(\tau)$ of output radiation pulse at $z = 12$ m for stepped axial profile of electron beam. Calculations have been performed with linear simulation code.

(a)

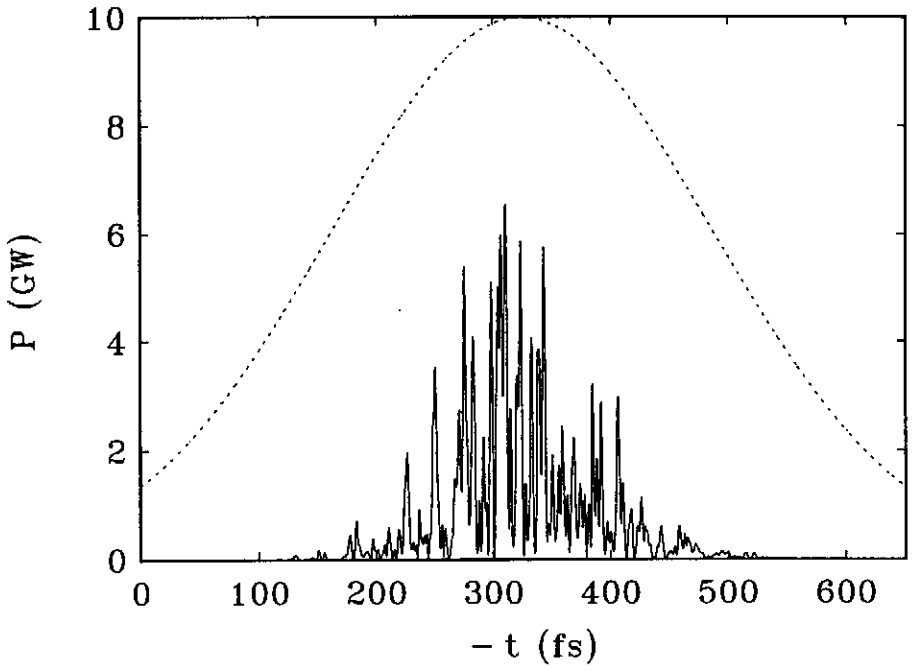

(b)

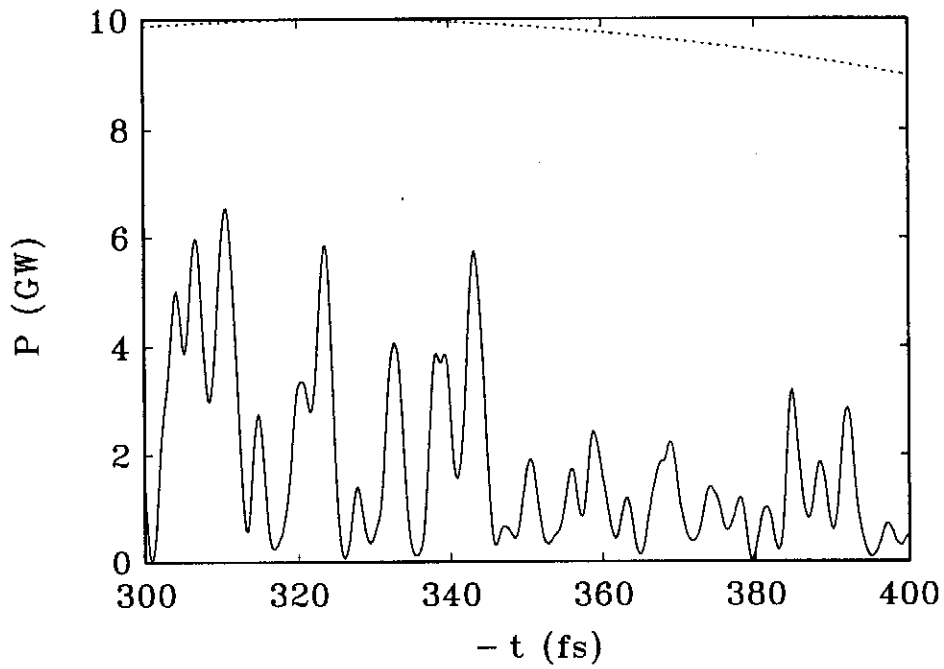

Fig. 5. Temporal structure of radiation pulse at $z = 12$ m for Gaussian axial profile of electron beam. Dash line presents the relative distribution of the electron beam current. Graph (a) is plotted over the full length of the electron beam and graph (b) presents enlarged fraction of graph (a). Calculations have been performed with linear simulation code.

(a)

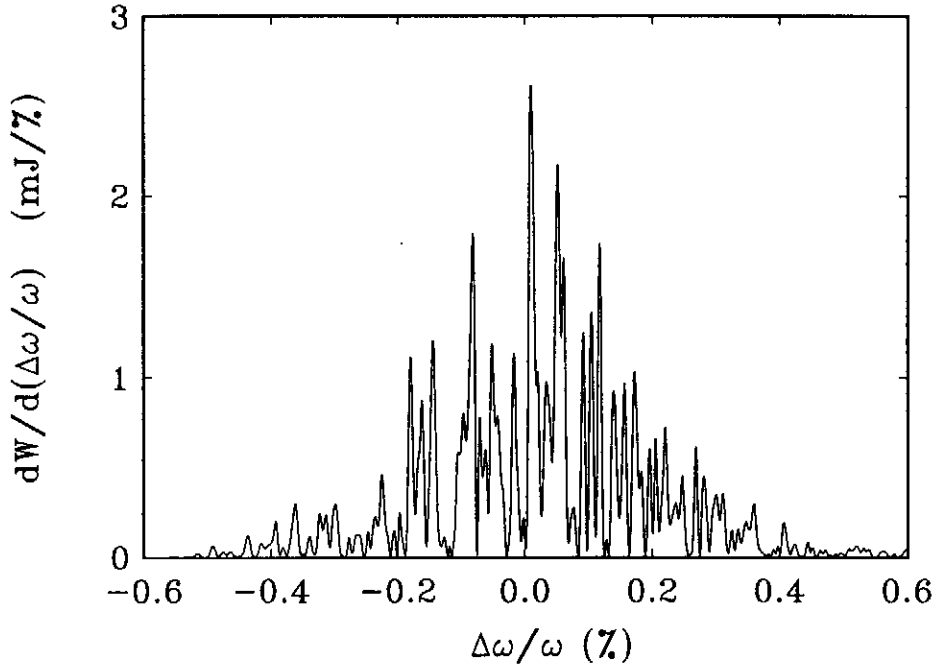

(b)

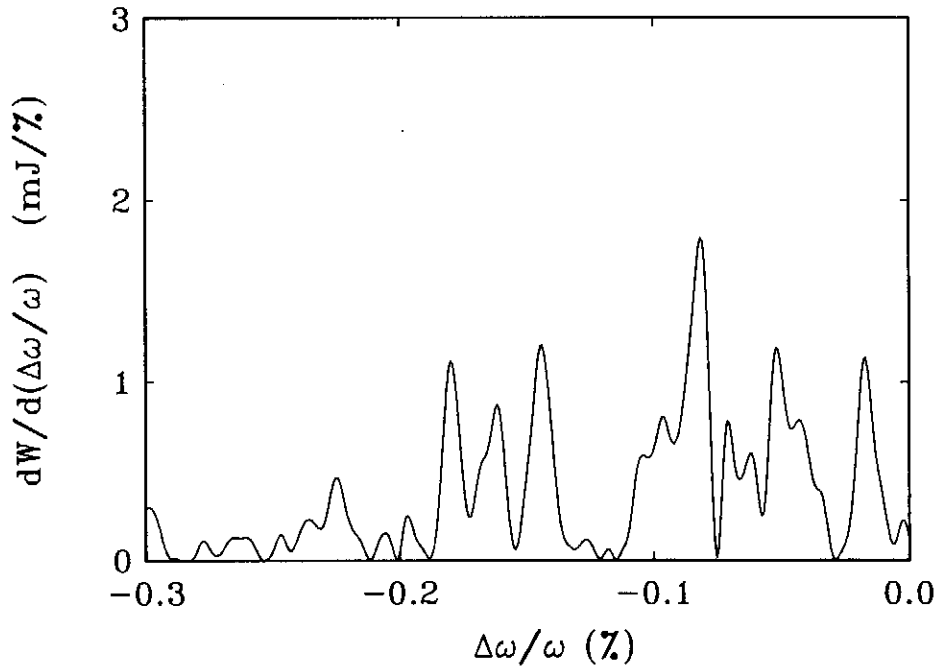

Fig. 6. Spectrum of radiation pulse at $z = 12$ m for Gaussian axial profile of electron beam. Graph (a) is plotted over the full length of the electron beam and graph (b) presents enlarged fraction of graph (a). Calculations have been performed with linear simulation code.

(a)

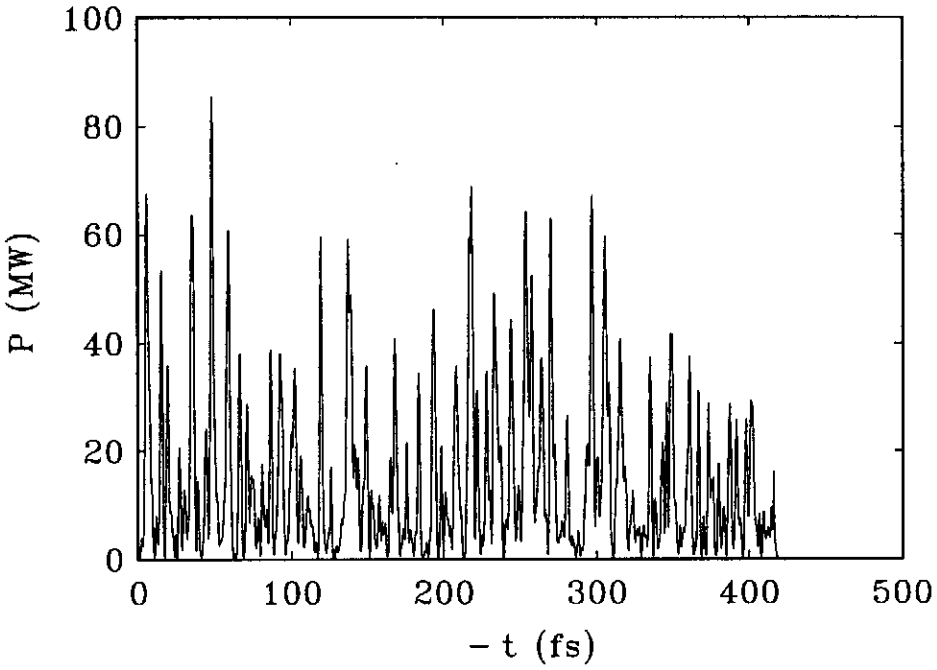

(b)

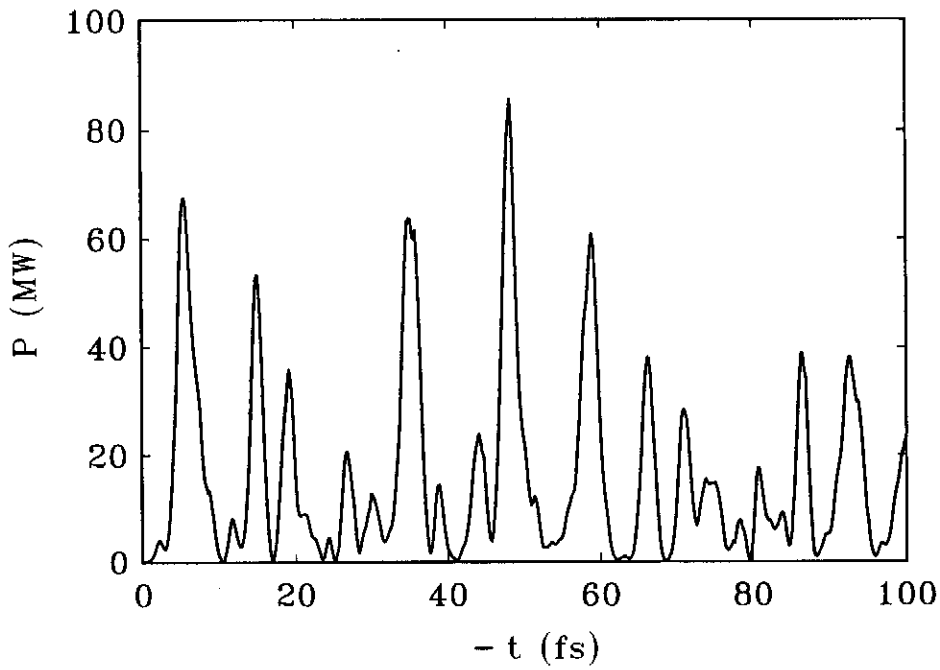

Fig. 7. Temporal structure of radiation pulse at $z = 9$ m for stepped axial profile of electron beam. Graph (a) is plotted over the full length of the electron beam and graph (b) presents enlarged fraction of graph (a). Calculations have been performed with nonlinear simulation code.

(a)

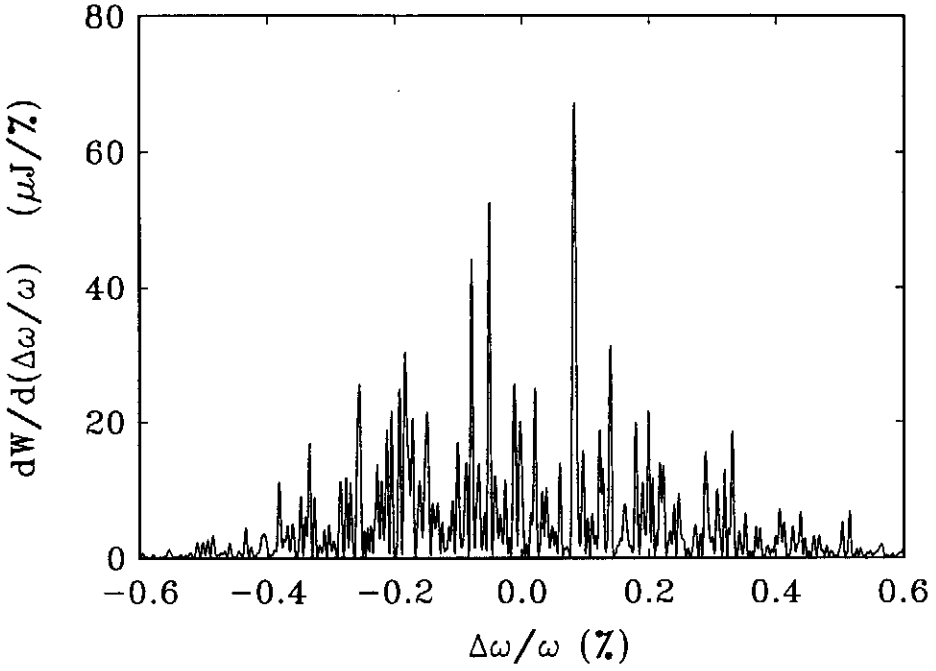

(b)

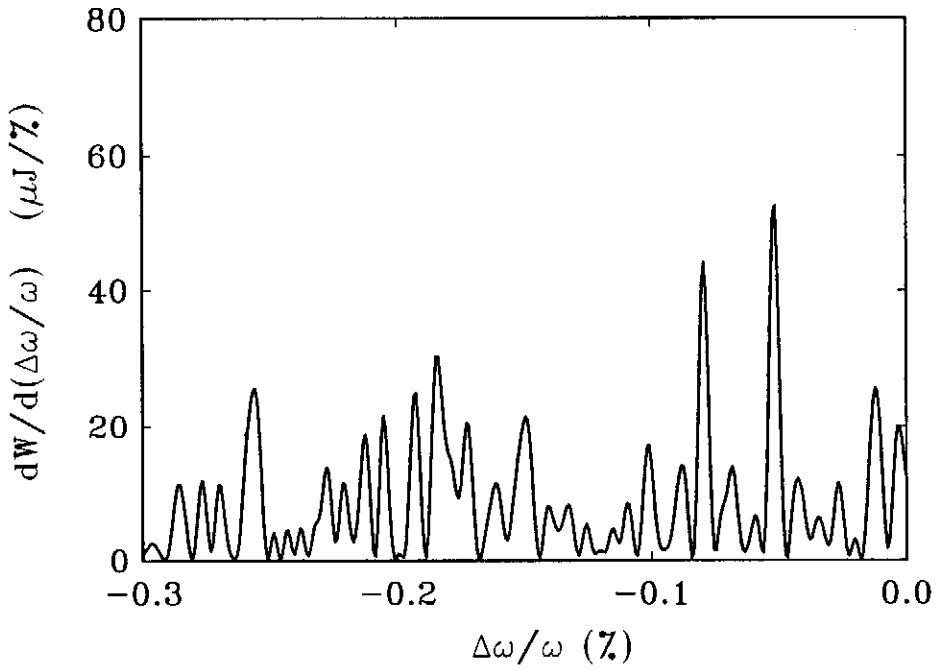

Fig. 8. Spectrum of radiation pulse at $z = 9$ m for stepped axial profile of electron beam. Graph (a) is plotted over the full length of the electron beam and graph (b) presents enlarged fraction of graph (a). Calculations have been performed with nonlinear simulation code.

(a)

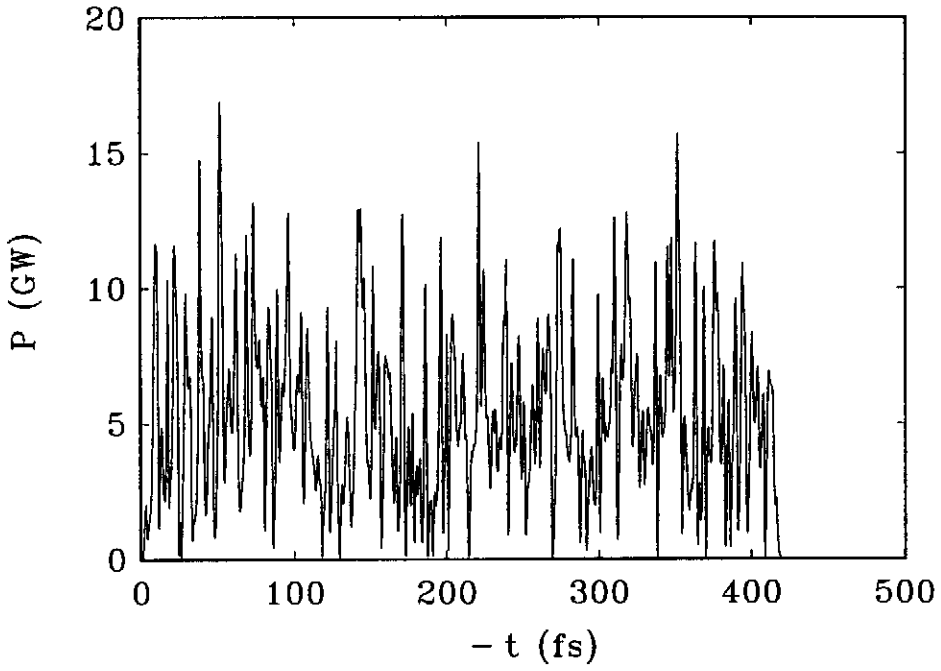

(b)

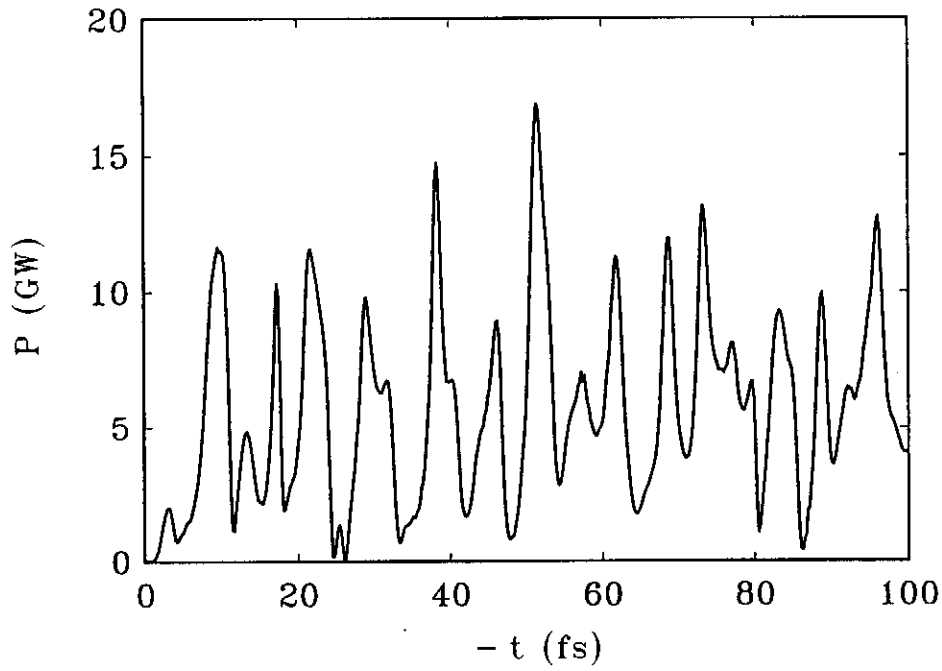

Fig. 9. Temporal structure of radiation pulse at $z = 14$ m (saturation point) for stepped axial profile of electron beam. Graph (a) is plotted over the full length of the electron beam and graph (b) presents enlarged fraction of graph (a). Calculations have been performed with nonlinear simulation code.

(a)

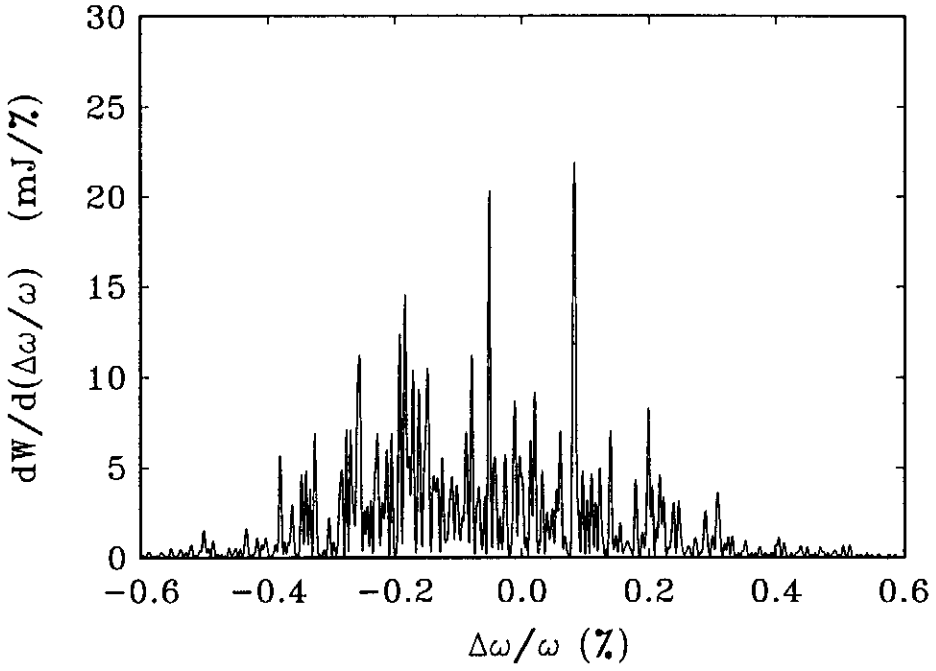

(b)

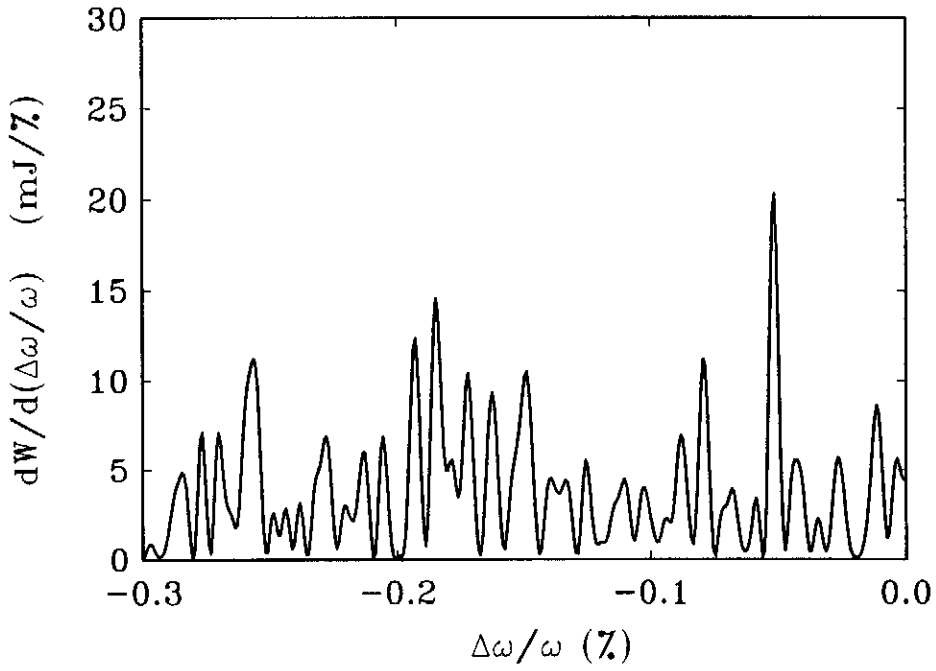

Fig. 10. Spectrum of radiation pulse at $z = 14$ m (saturation point) for stepped axial profile of electron beam. Graph (a) is plotted over the full length of the electron beam and graph (b) presents enlarged fraction of graph (a). Calculations have been performed with nonlinear simulation code.

(a)

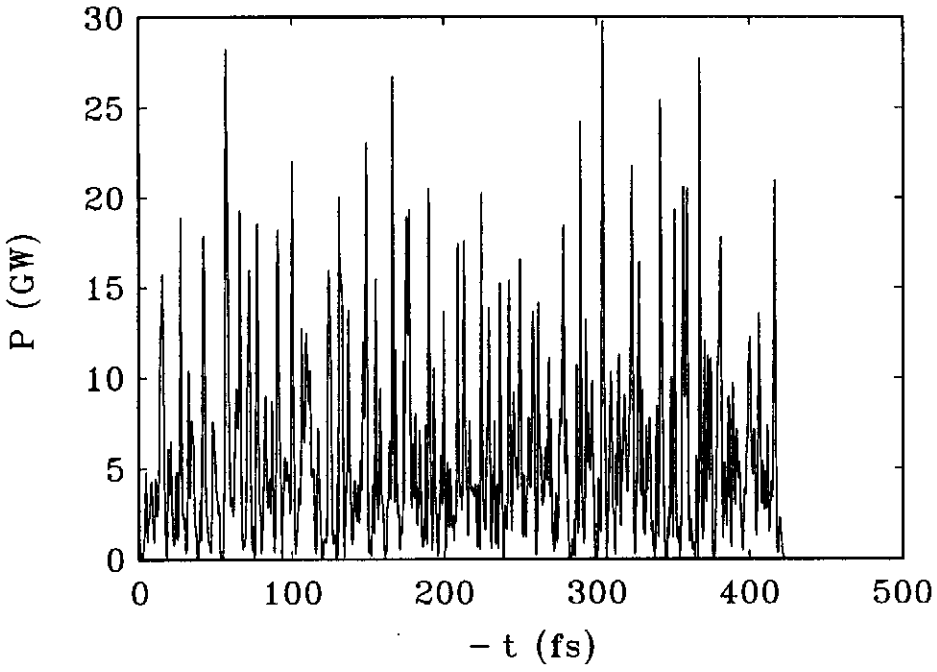

(b)

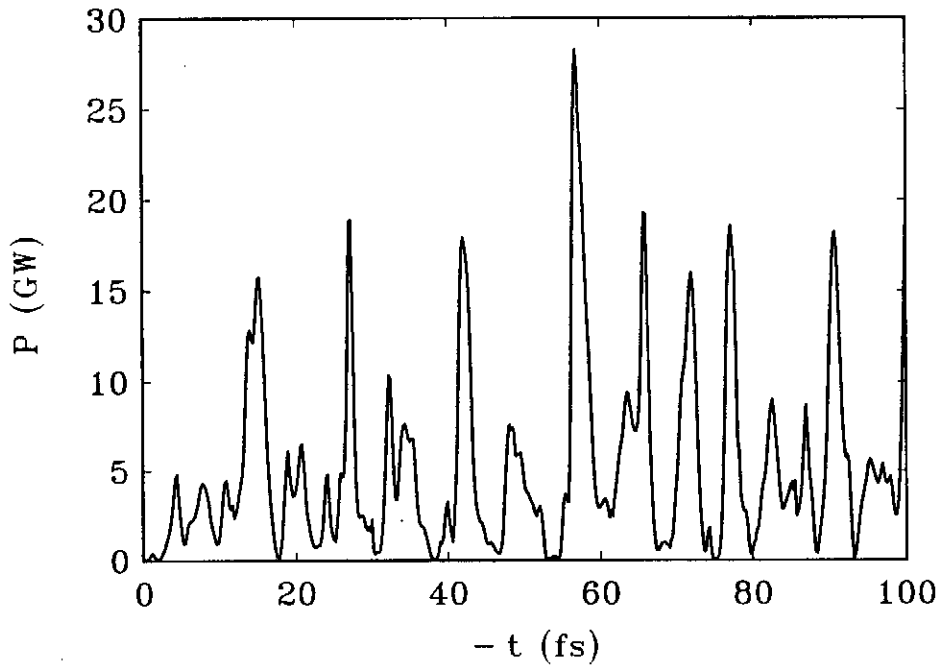

Fig. 11. Temporal structure of radiation pulse at $z = 19$ m for stepped axial profile of electron beam. Graph (a) is plotted over the full length of the electron beam and graph (b) presents enlarged fraction of graph (a). Calculations have been performed with nonlinear simulation code.

(a)

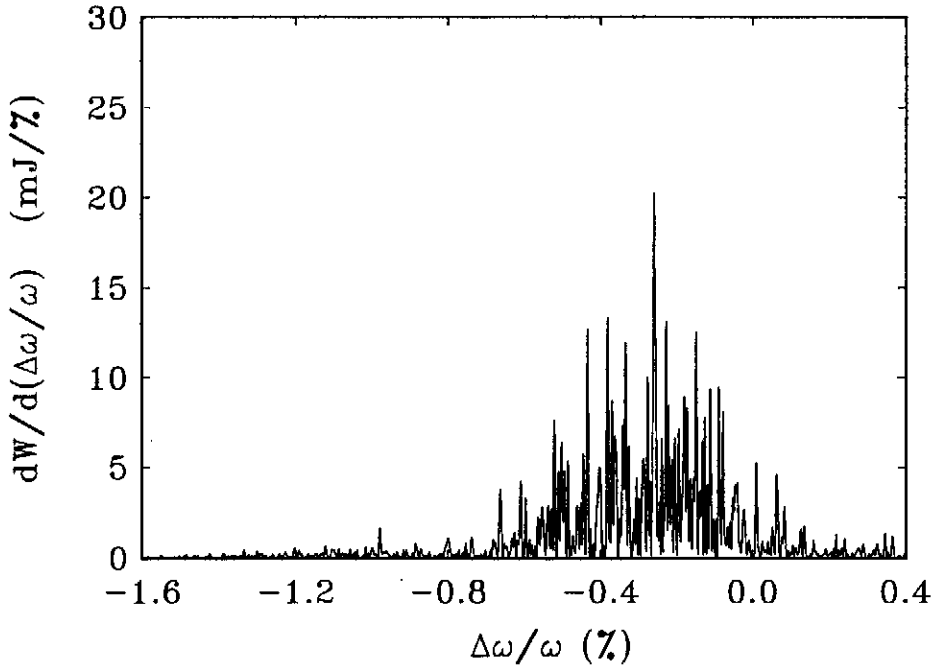

(b)

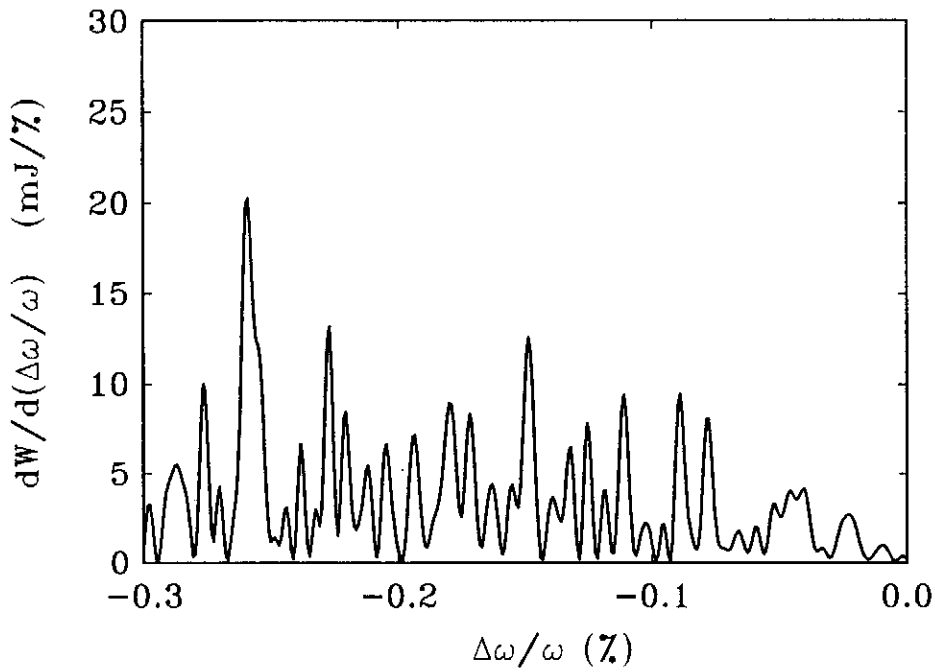

Fig. 12. Spectrum of radiation pulse at $z = 19$ m for stepped axial profile of electron beam. Graph (a) is plotted over the full length of the electron beam and graph (b) presents enlarged fraction of graph (a). Calculations have been performed with nonlinear simulation code.

(a)

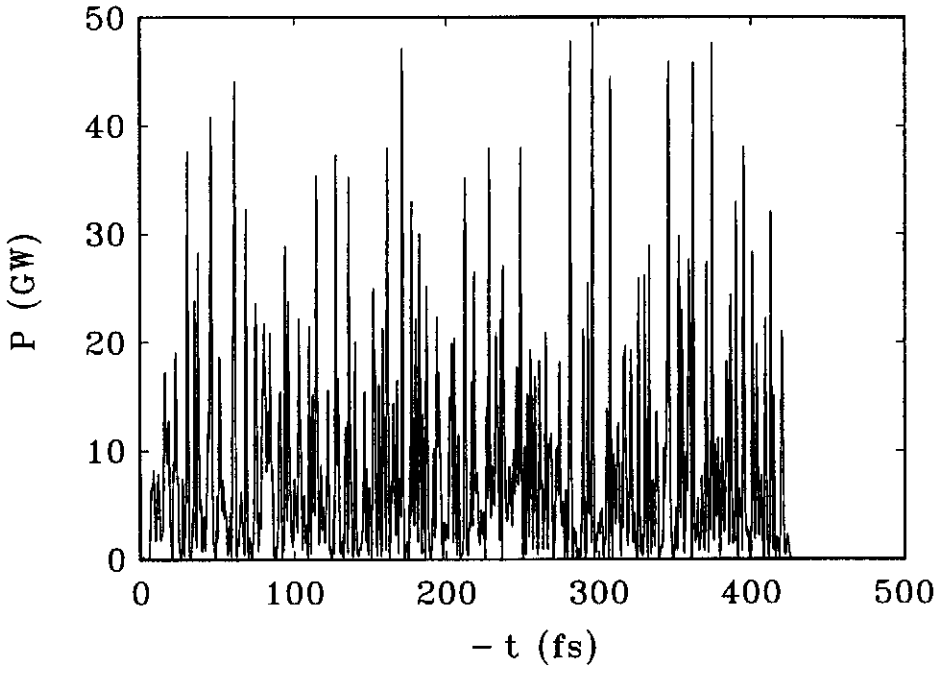

(b)

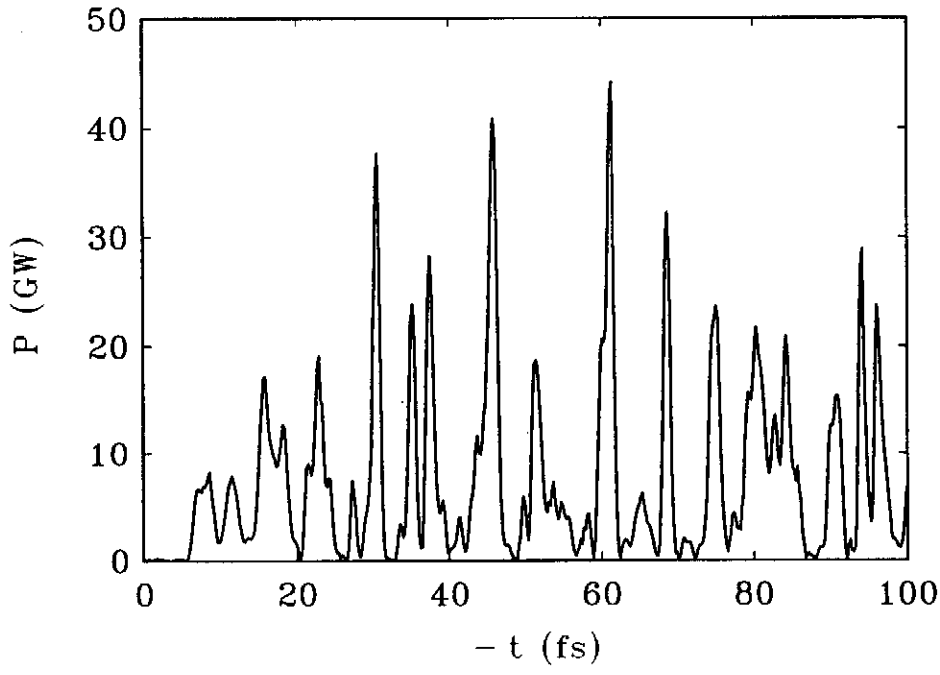

Fig. 13. Temporal structure of radiation pulse at $z = 24$ m for stepped axial profile of electron beam. Graph (a) is plotted over the full length of the electron beam and graph (b) presents enlarged fraction of graph (a). Calculations have been performed with nonlinear simulation code.

(a)

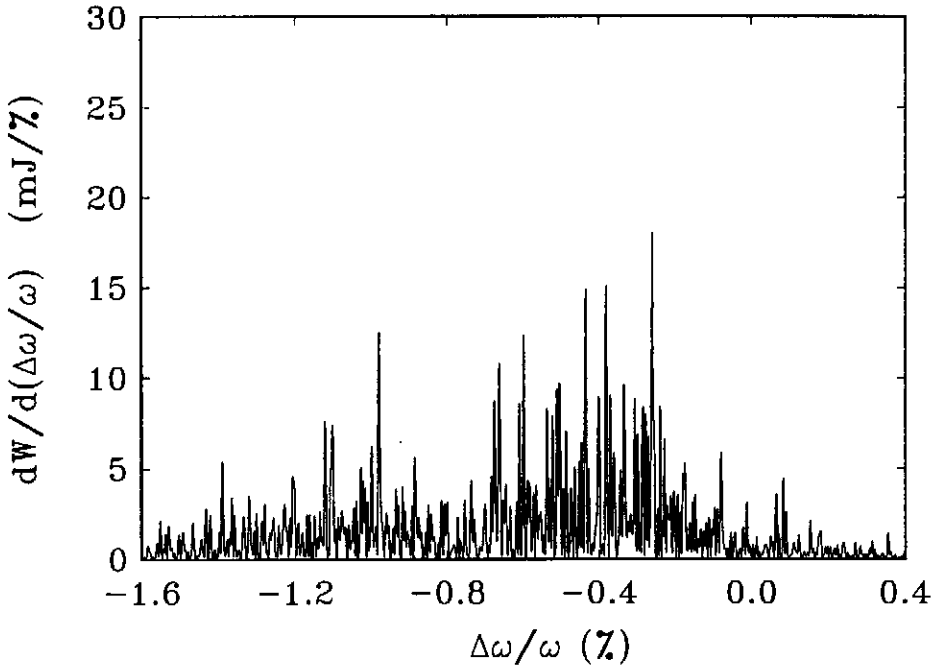

(b)

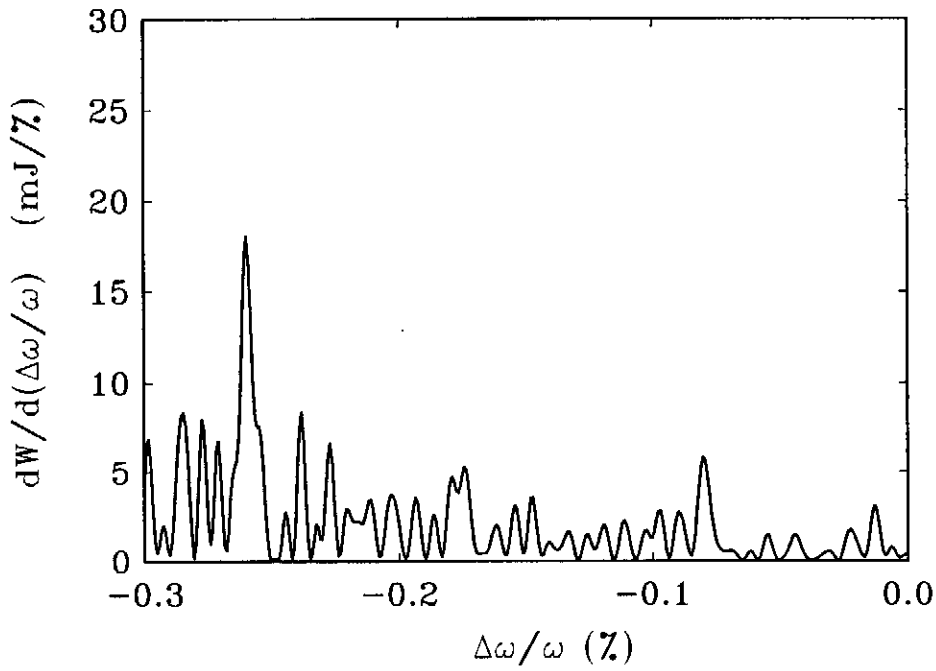

Fig. 14. Spectrum of radiation pulse at $z = 24$ m for stepped axial profile of electron beam. Graph (a) is plotted over the full length of the electron beam and graph (b) presents enlarged fraction of graph (a). Calculations have been performed with nonlinear simulation code.

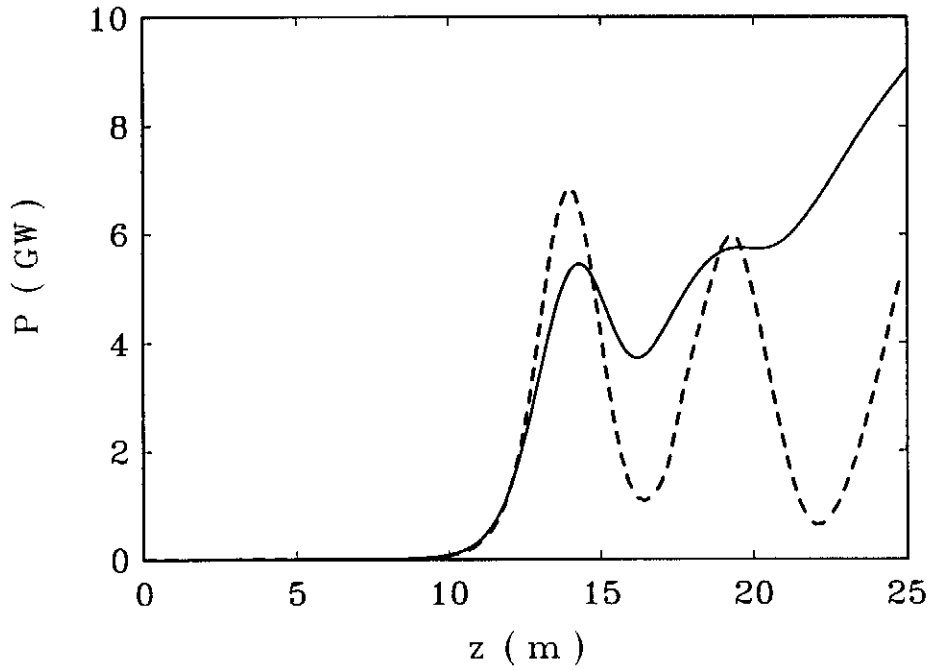

Fig. 15. Dependence of the radiation power (averaged over pulse) on the undulator length for the case of stepped axial profile of electron beam. Dotted line is calculated with steady-state code at 100 W input radiation power. Calculations have been performed with nonlinear simulation code.

(a)

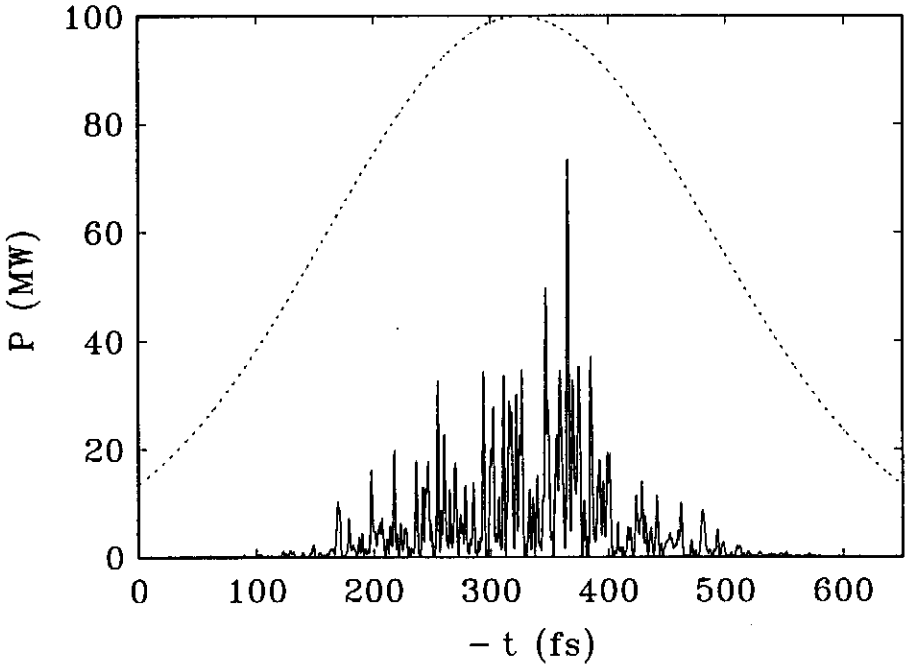

(b)

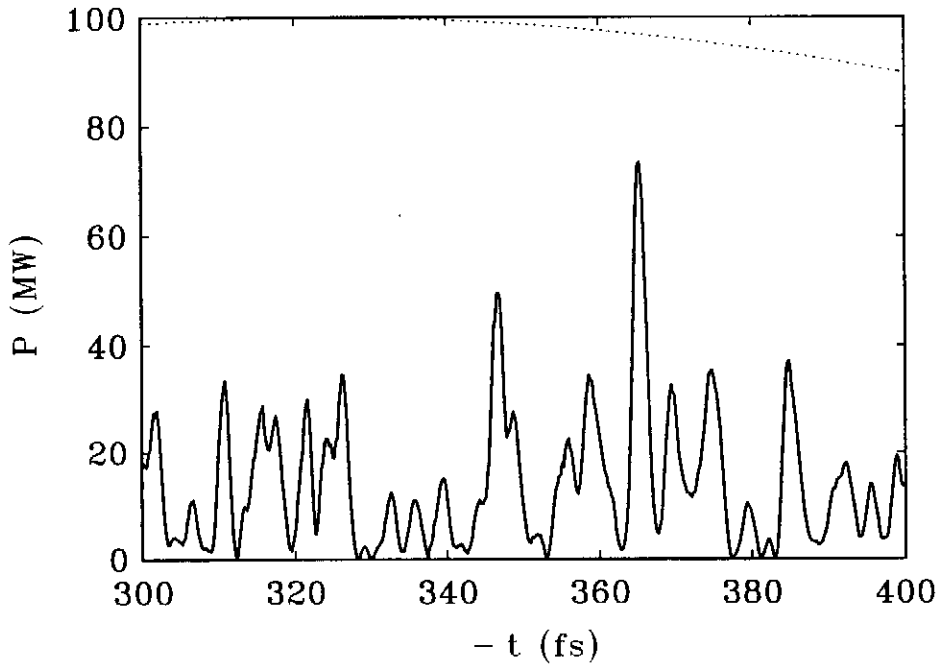

Fig. 16. Temporal structure of radiation pulse at $z = 9$ m for Gaussian axial profile of electron beam. Graph (a) is plotted over the full length of the electron beam and graph (b) presents enlarged fraction of graph (a). Dashed line presents relative distribution of the electron beam current. Calculations have been performed with nonlinear simulation code.

(a)

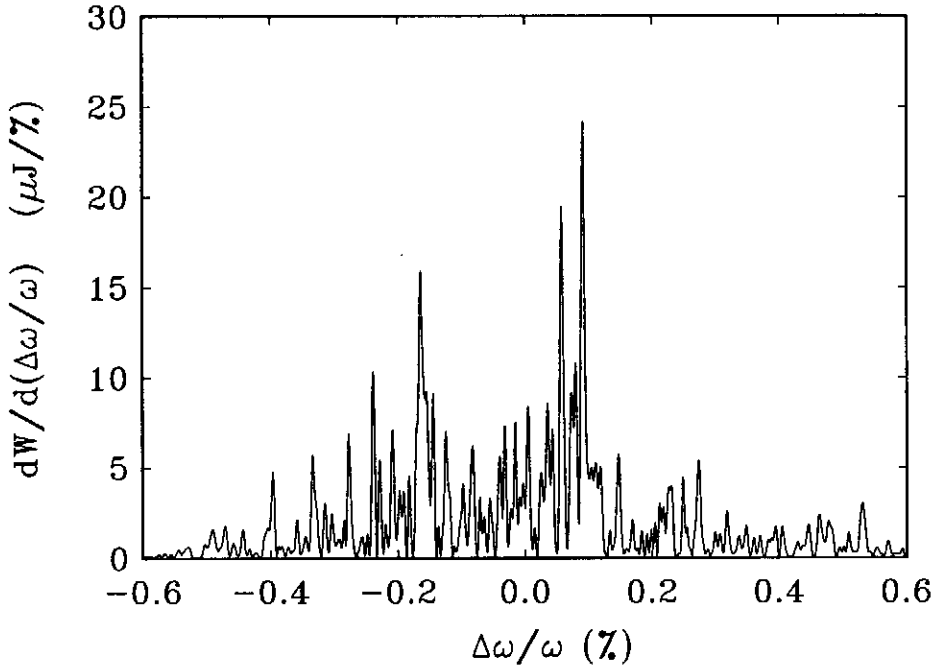

(b)

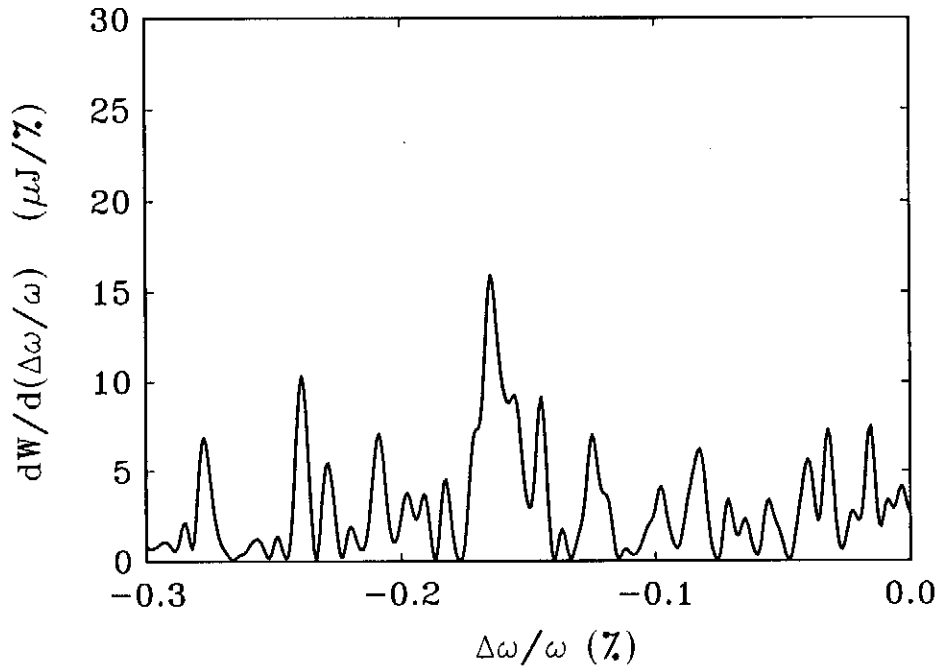

Fig. 17. Spectrum of radiation pulse at $z = 9$ m for Gaussian axial profile of electron beam. Graph (a) is plotted over the full length of the electron beam and graph (b) presents enlarged fraction of graph (a). Dashed line presents relative distribution of the electron beam current. Calculations have been performed with nonlinear simulation code.

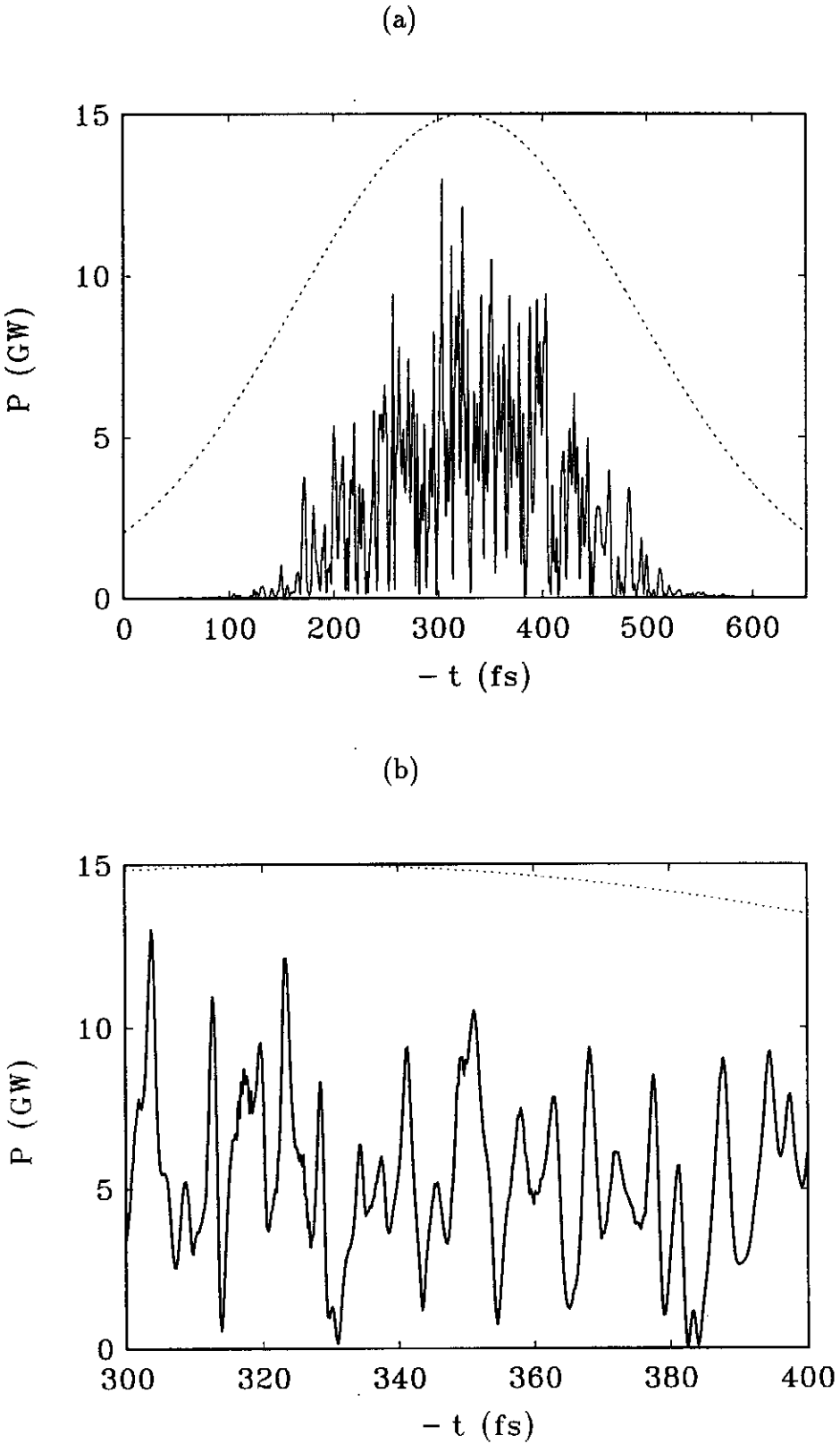

Fig. 18. Temporal structure of radiation pulse at $z = 14$ m for Gaussian axial profile of electron beam. Graph (a) is plotted over the full length of the electron beam and graph (b) presents enlarged fraction of graph (a). Dashed line presents relative distribution of the electron beam current. Calculations have been performed with nonlinear simulation code.

(a)

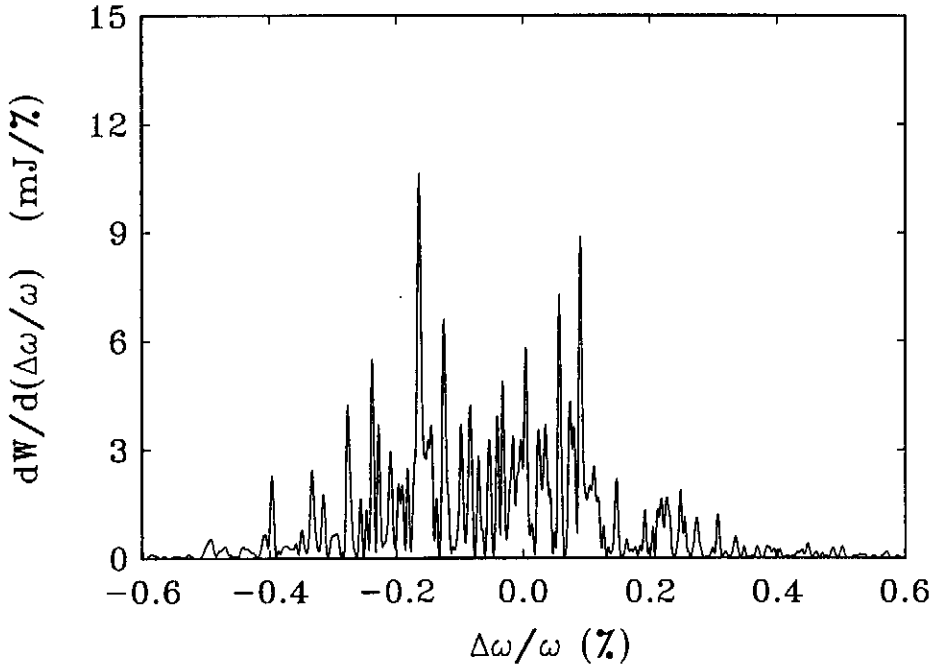

(b)

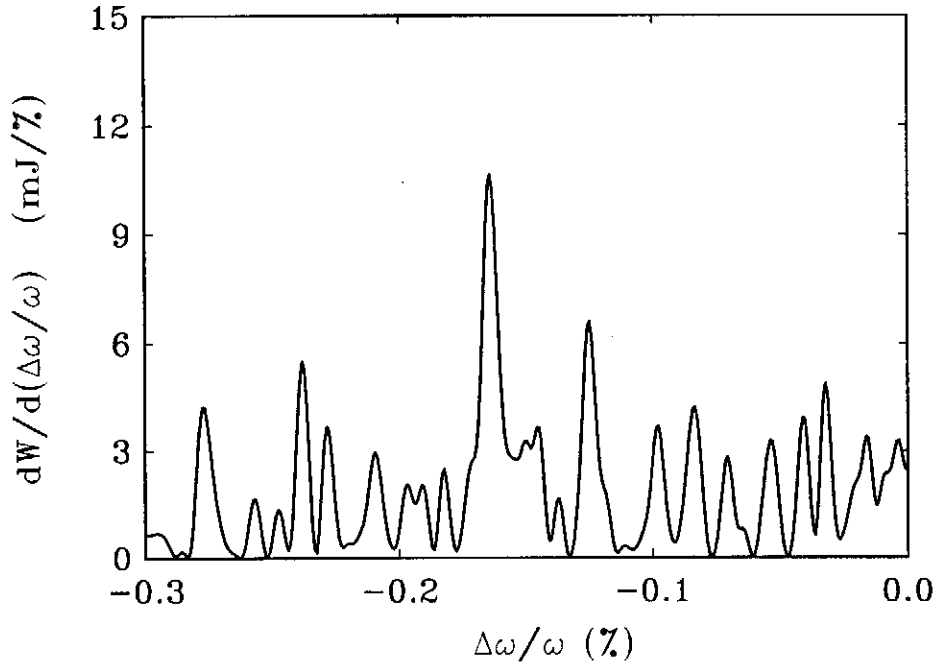

Fig. 19. Spectrum of radiation pulse at z = 14 m for Gaussian axial profile of electron beam. Graph (a) is plotted over the full length of the electron beam and graph (b) presents enlarged fraction of graph (a). Dashed line presents relative distribution of the electron beam current. Calculations have been performed with nonlinear simulation code.

(a)

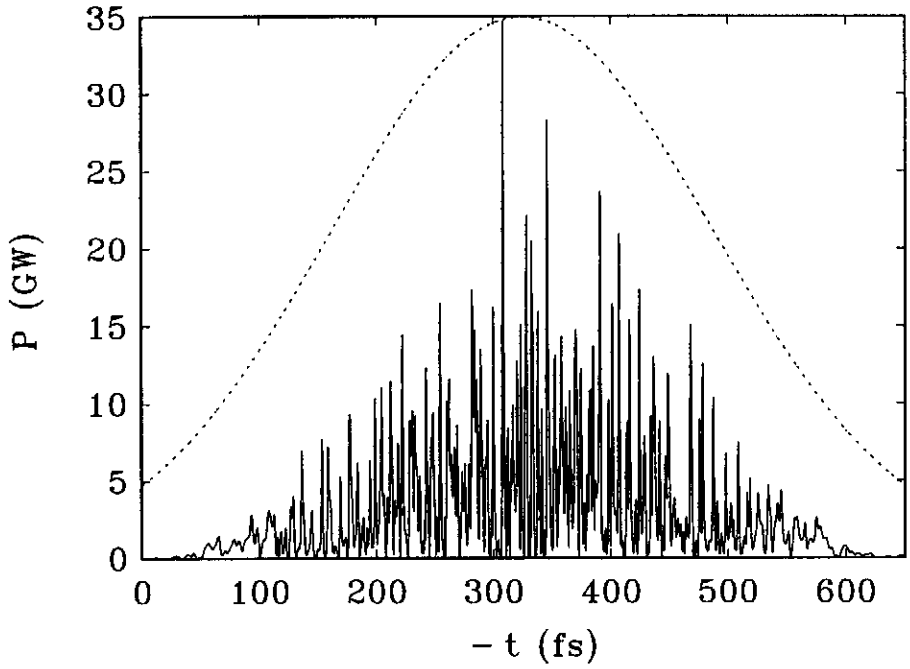

(b)

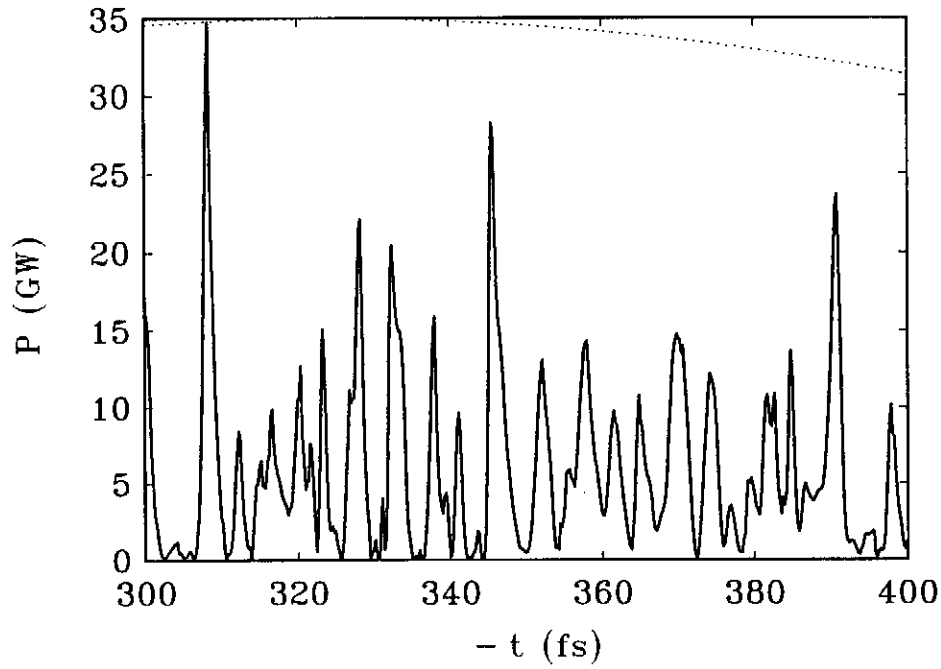

Fig. 20. Temporal structure of radiation pulse at $z = 19$ m for Gaussian axial profile of electron beam. Graph (a) is plotted over the full length of the electron beam and graph (b) presents enlarged fraction of graph (a). Dashed line presents relative distribution of the electron beam current. Calculations have been performed with nonlinear simulation code.

(a)

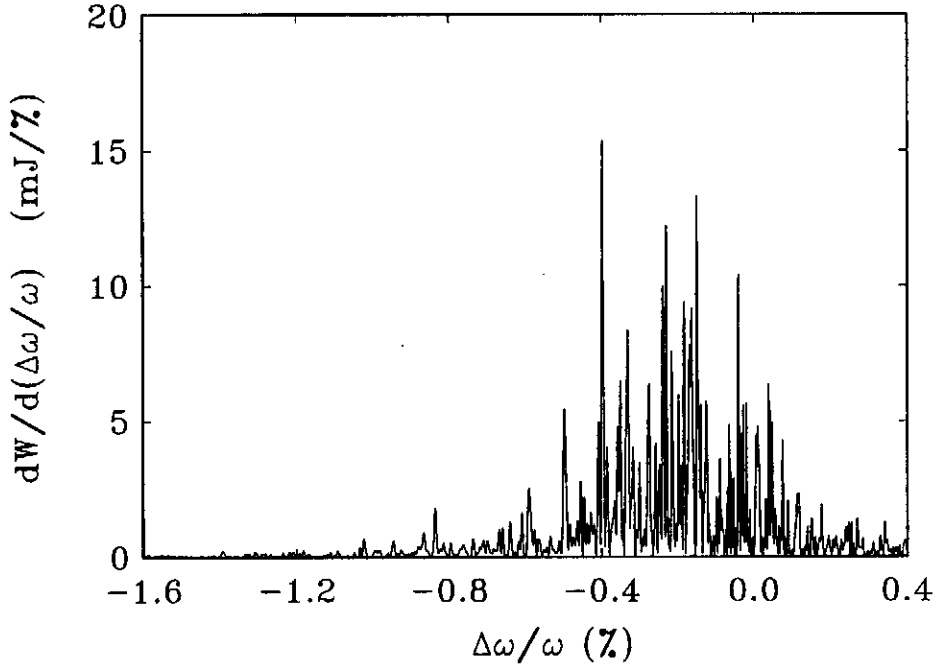

(b)

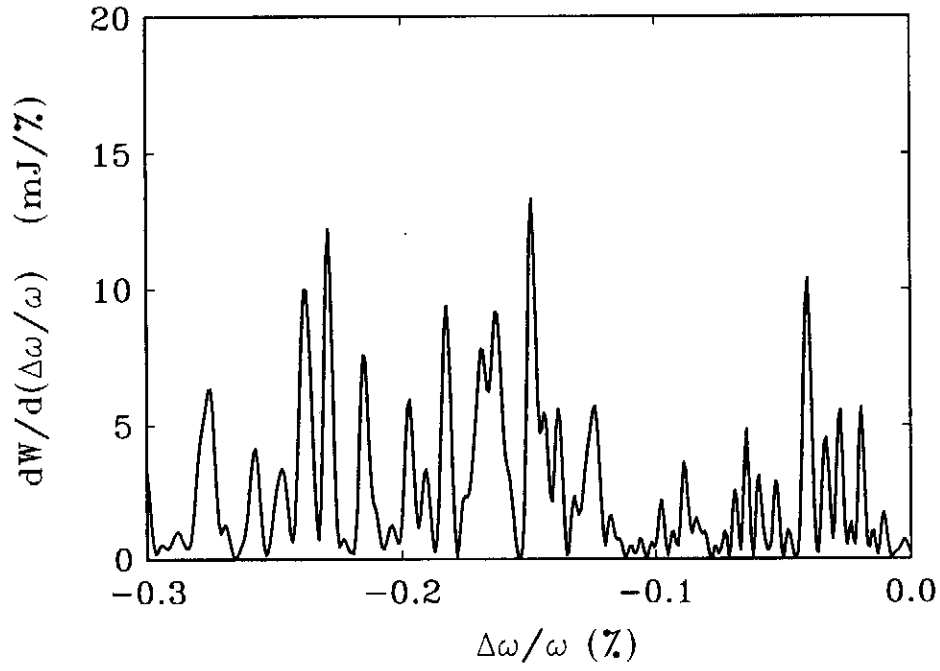

Fig. 21. Spectrum of radiation pulse at z = 19 m for Gaussian axial profile of electron beam. Graph (a) is plotted over the full length of the electron beam and graph (b) presents enlarged fraction of graph (a). Dashed line presents relative distribution of the electron beam current. Calculations have been performed with nonlinear simulation code.

(a)

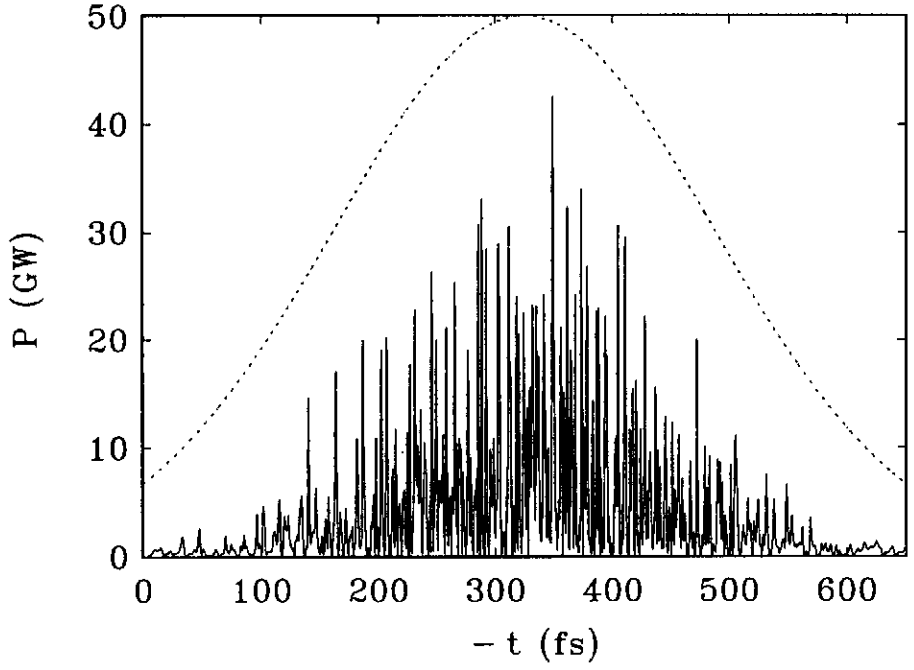

(b)

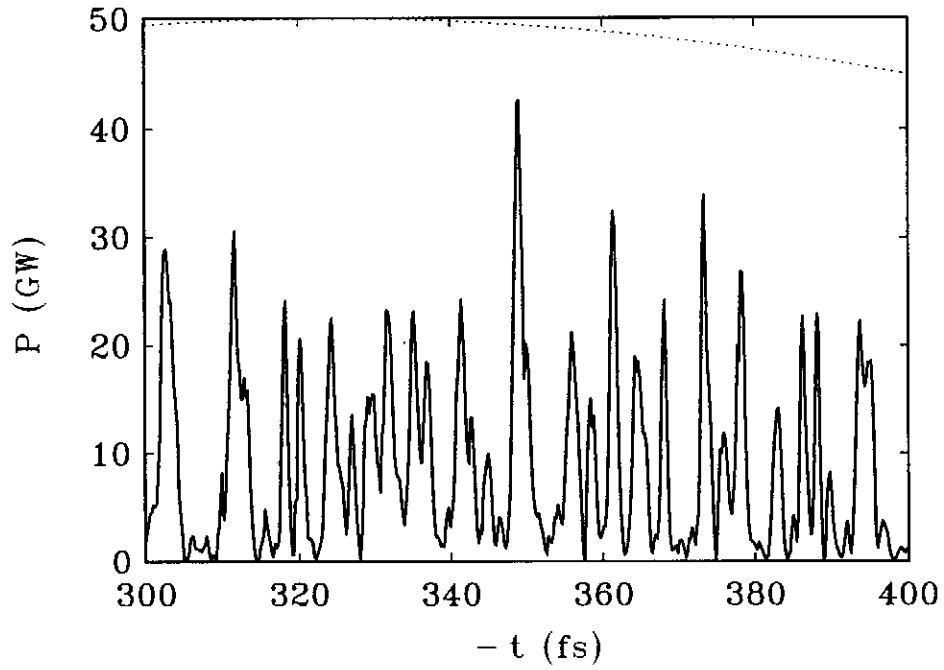

Fig. 22. Temporal structure of radiation pulse at $z = 24$ m for Gaussian axial profile of electron beam. Graph (a) is plotted over the full length of the electron beam and graph (b) presents enlarged fraction of graph (a). Dashed line presents relative distribution of the electron beam current. Calculations have been performed with nonlinear simulation code.

(a)

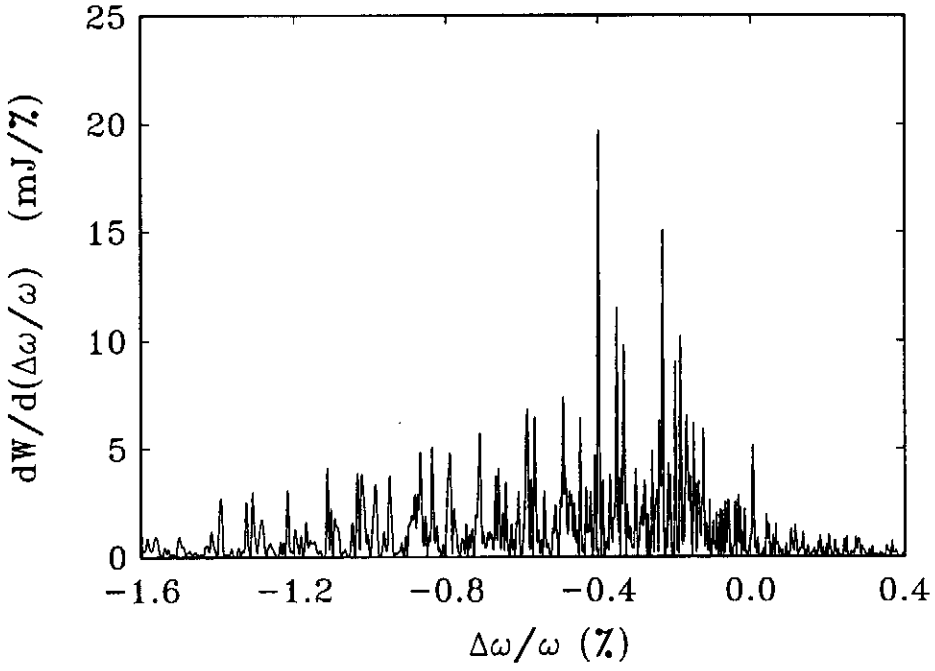

(b)

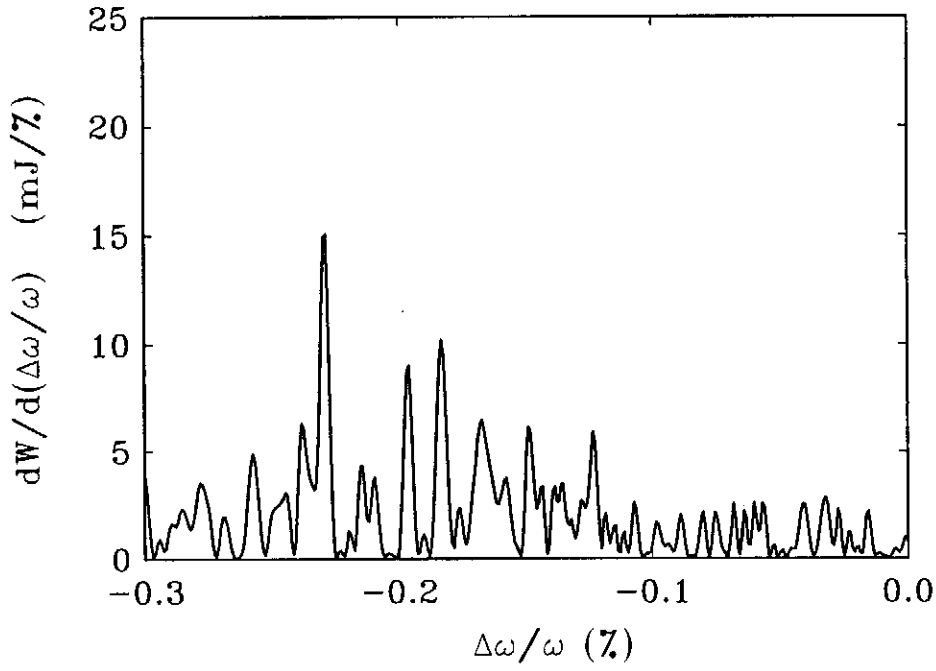

Fig. 23. Spectrum of radiation pulse at $z = 24$ m for Gaussian axial profile of electron beam. Graph (a) is plotted over the full length of the electron beam and graph (b) presents enlarged fraction of graph (a). Dashed line presents relative distribution of the electron beam current. Calculations have been performed with nonlinear simulation code.

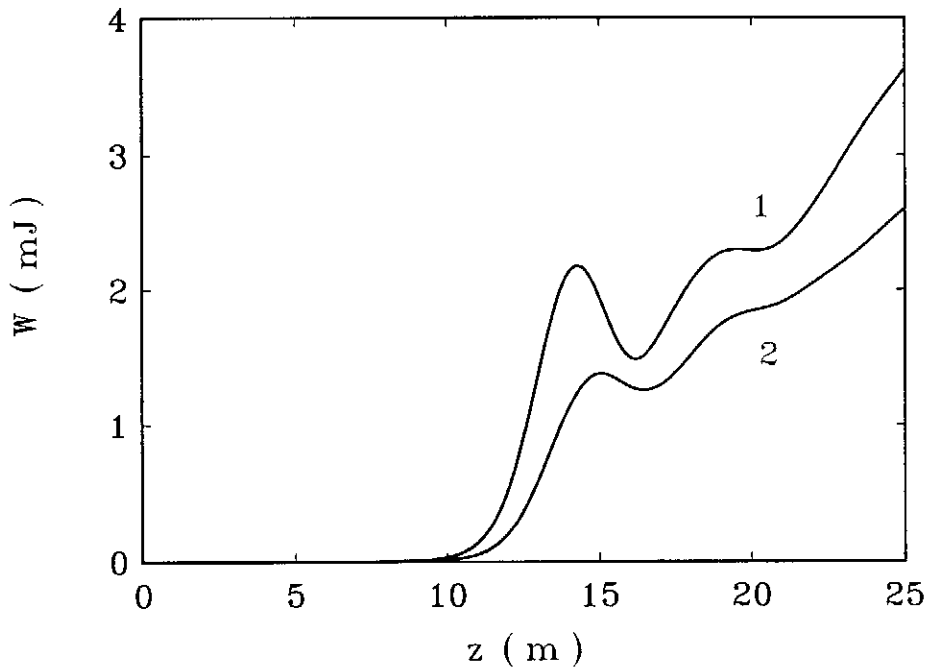

Fig. 24. Dependence of the radiation flash energy on the undulator length for the stepped (curve 1) and Gaussian (curve 2) axial profile of electron beam. Calculations have been performed with nonlinear simulation code.